AD_____

Award Number: W81XWH-08-1-0358

TITLE: Multiadaptive Plan (MAP) IMRT to Accommodate Independent Movement of the Prostate and Pelvic Lymph Nodes

PRINCIPAL INVESTIGATOR: Ping Xia, Ph.D.

CONTRACTING ORGANIZATION: The Cleveland Clinic Foundation
Cleveland, OH 44195

REPORT DATE: December 2011

TYPE OF REPORT: Annual

PREPARED FOR: U.S. Army Medical Research and Materiel Command
Fort Detrick, Maryland 21702-5012

REPORT DOCUMENTATION PAGE

Form Approved
OMB No. 0704-0188

1. REPORT DATE *(DD-MM-YYYY)*	2. REPORT TYPE	3. DATES COVERED *(From - To)*
01-12-2011	Annual	1 MAY 2010 -12 NOV 2011

4. TITLE AND SUBTITLE

Multiadaptive Plan (MAP) IMRT to Accommodate Independent Movement of the Prostate and Pelvic Lymph Nodes

5a. CONTRACT NUMBER

5b. GRANT NUMBER
W81XWH-08-1-0358

5c. PROGRAM ELEMENT NUMBER

6. AUTHOR(S)

Ping Xia, Ph.D.

E-Mail: xiap@ccf.org

5d. PROJECT NUMBER

5e. TASK NUMBER

5f. WORK UNIT NUMBER

7. PERFORMING ORGANIZATION NAME(S) AND ADDRESS(ES)

The Cleveland Clinic Foundation
Cleveland, OH 44195

8. PERFORMING ORGANIZATION REPORT NUMBER

9. SPONSORING / MONITORING AGENCY NAME(S) AND ADDRESS(ES)

U.S. Army Medical Research and Materiel Command
Fort Detrick, Maryland 21702-5012

10. SPONSOR/MONITOR'S ACRONYM(S)

11. SPONSOR/MONITOR'S REPORT NUMBER(S)

12. DISTRIBUTION / AVAILABILITY STATEMENT

Approved for Public Release; Distribution Unlimited

13. SUPPLEMENTARY NOTES

14. ABSTRACT

We found that the rotational shifts detected by aligning implanted markers between the planning images and the verification images may not determine the true rotation of the prostate. Ignoring these detected rotational shifts may lead to erroneous errors of localizing the prostate. We found that the prostate rotation can be compensated with corrections made in translational shifts, achieving improved geometric and dosimetric evaluation indices. Furthermore, we found that when the verification images had the same quality as the planning computed tomography (CT), the use of patient-specific atlas could produce automatic contours that were highly consistent with the manually contoured ones. Performance of patient-specific atlas is drastically better than the results of general patient population-based atlas as reported last year.

15. SUBJECT TERMS

Adaptive Radiotherapy, Image guided Radiotherapy, Prostate cancer, Pelvic Lymph nodes

16. SECURITY CLASSIFICATION OF:			17. LIMITATION OF ABSTRACT	18. NUMBER OF PAGES	19a. NAME OF RESPONSIBLE PERSON
a. REPORT	b. ABSTRACT	c. THIS PAGE			USAMRMC
U	U	U	UU	75	19b. TELEPHONE NUMBER *(include area code)*

Table of Contents

Introduction

It is estimated that 40% or more of patients with intermediate-to-high risk prostate cancer will relapse locally and systemically within five years after definitive radiotherapy. We hypothesize that this high rate of failure is partly due to under-irradiation of the pelvic lymph nodes. One of the challenges to using IMRT in concurrent treatment of the prostate and the pelvic lymph nodes is the independent movement of the prostate relative to the lymph nodes, rendering the conventional iso-center shifting method of tracking prostate movement inadequate. The purpose of this research is to develop a novel method using multi-adaptive plan (MAP) IMRT to accommodate independent movement of the two targeted tumor volumes. In order to evaluate effectiveness of the MAP IMRT approach, we first establish a baseline benchmark by creating a set of ideal IMRT plans for each patient based on the daily acquired mega-voltage or kilo-voltage cone beam computed tomography (CT), which represents the ideal case of daily online treatment planning. Based on this established benchmark, we can further evaluate two adaptive strategies: strategy A creates a set of IMRT plans individually optimizing on a series of possible prostate positions in the planning CT; and strategy B creates a set of multi-adaptive plans by dynamically adjusting the radiation apertures to accommodate the daily position of the prostate.

Body

(a) Task 1 (3) –Patterns of prostate motion and effect of prostate rotation

As we mentioned in last year's report**,** we encountered large rotations in the prostates of 8 patients when aligning the implanted markers as stated in Task 1. Due to the limited soft tissue contrast of mega-voltage cone beam CT (MV- CBCT, the source of the rotation, migration of the marker, or true rotation of the prostate, could not be determined. From an IRB approved registry of prostate cancer at Cleveland Clinic, we identified five patients, with 43 kilo-voltage cone beam CT (KV-CBCT) and implanted markers. With these KV-CBCTs, for which the image quality had sufficient soft tissue contrast, we were able to manually delineate the prostate, bladder, and rectum on each CBCT. To eliminate potential setup errors, we first co-registered each CBCT with its corresponding planning CT based on the pelvic bony alignment. These shifts were subtracted from all shifts discussed below. Therefore, the registration shifts for the remaining context represent the prostate displacements relative to the bone.

Table I. Prostate rotational shift variations in degrees.

	LR (degree)	AP (degree)	SI (degree)
Overall mean	3.3	-1.4	-0.8
Overall SD*	5.8	2.9	2.8
Systematic SD*	4.6	2.3	2.1
Random SD*	4.1	2.0	2.0

SD*= standard deviation; LR = Left and Right; AP = anterior and posterior;
SI = superior and inferior

When co-registering three implanted markers from a CBCT with those in the planning CT, an unique solution can be determined analytically with three translational shifts and three rotational shifts while considering three implanted markers as three points. With this analytical method, a computer program can automatically determine the rotation shifts of the prostate in each CBCT. As shown in Table 1, we found that prostate rotational shifts dominated in the left-right axis, with respective systematic and random components of 4.6° and 4.1°. Figure 1 shows the detailed prostate rotational shifts along three principal axes for 43 CBCT analyzed and the frequency distributions of the rotational shifts along these three axes.

Without a robotic treatment table (or six degree freedom), correcting these rotational errors were not clinically feasible thus often being ignored while assuming they were small. Our data showed that this assumption may not be valid as some rotational shifts could be greater than 10°. To quantify the geometric and dosimetric effect of ignoring these rotational shifts, we compared two marker registration methods. One method allowed both translational and rotational shifts to align the markers first and then zero out the rotation, mimicking the frequent clinical practice in situations without a six-degree treatment table. The other method allowed only translational shifts to align markers, partially compensating the prostate rotations by translational shifts. When the rotational shifts were greater than 10°, we found that the differences in the prostate of center of mass distance (CMD) between the two marker registrations were greater than 5 mm in 85.7% of these fractions; when the rotational shifts were greater than 6°, the differences of CMD were greater than 4 mm in 61.1% of these fractions.

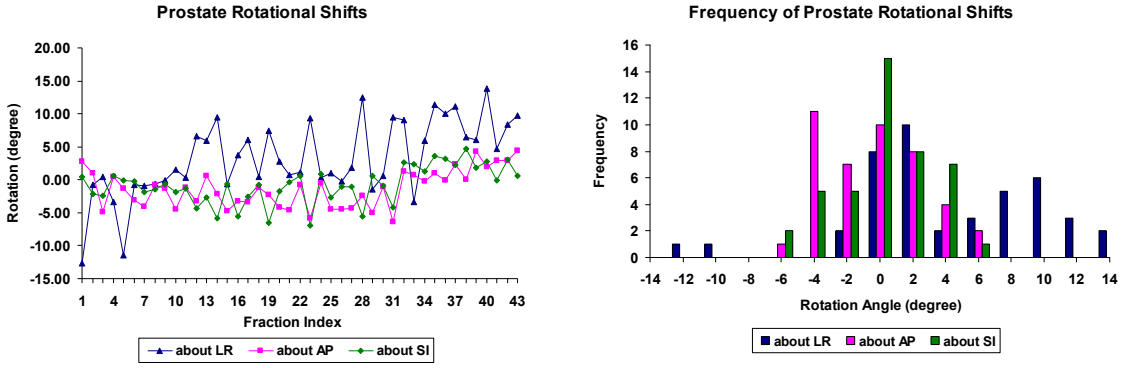

(a) (b)

Figure 1. (a) Detailed prostate rotational shifts along three principal axes; (b) Frequency distributions of the rotational shifts along these three axes.

To determine which marker registration method is more accurate, we use the prostate contour registration method as a benchmark. With contour-based registration, we manually align the contour of the prostate on the CBCT with the contour of the prostate on the planning CT while maximizing the overlap of the two contours with translational shifts. This method inherently compensates the prostate rotational errors into the translational shifts. When compared to the contoure- based registration, the mean CMD difference of the marker registration without rotation compensation was 6.6 mm (range from 1.9 mm to 15.8 mm). The mean CMD difference of the marker registration with rotation compensation was smaller, 3.9 mm (range from 1.1 mm to 9.1 mm). Figure 2 illustrates the differences among these registration methods. In Figure 4, there are four different prostate contours: (a) prostate contour transferred from the planning CT after the marker-based registration without rotation

compensation; (b) prostate contour transferred from the planning CT after the marker registration with rotation compensation; (c) prostate contour transferred from the planning CT after contour based registration; (d) the prostate contour directly delineated on the CBCT. The transferred prostate contour from the contour registration may minimize potential deviation of the prostate delineation on the KV-CBCT due to the limited soft tissue contrast despite its improvement when compared to mega-voltage (MV) CBCT. For the following geometry and dosimetric analyses, we used transferred prostate contour after contour registration as the "prostate of the day". As shown in Figure 3, the difference in the center of the mass of the transferred prostate contour after contour registration and the center of the mass of the prostate contour manually drawn on the CBCT were small, with an average of 1.3 ± 0.5 mm.

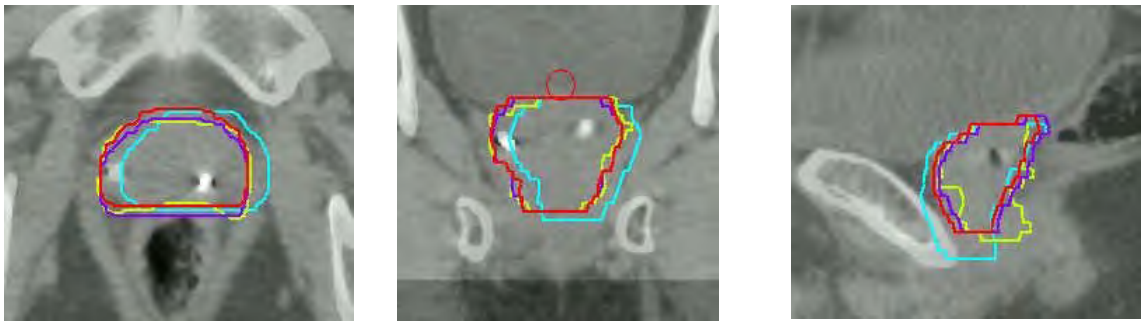

(a) (b) (c)

Figure 2. Prostate contours on a CBCT obtained from different registration methods in (a) transverse, (b) coronal, and (c) sagittal views. The outline in blue is the prostate contour transferred from the planning CT after the marker registration without rotation compensation; the outline in red is transferred from the planning CT after the marker registration with rotation compensation; the outline in purple is transferred from the planning CT after contour-based registration; the outline in yellow is the manual contour of the prostate directly on the CBCT.

The analysis of OI showed that, to achieve 95% overlap between the "prostate at planning" and the "prostate of the day", marker registration with translational compensation can reduce a planning margin reduction of 2mm in 3 out of 5 patients (66.7%). Dosimetrically, with 2 mm planning margin reduction, the average daily dose to 95% of the prostate (D95) were 1.97 Gy and 1.91 Gy for the marker-based registration methods with and without compensation, respectively ($p = 0.03$).

In conclusion, compensating for the rotations with translational shifts is possible, and it will improve geometric and dosimetric indices when the prostate rotation cannot be corrected by a means of a six degree treatment couch. A completed manuscript is attached in Appendix A.

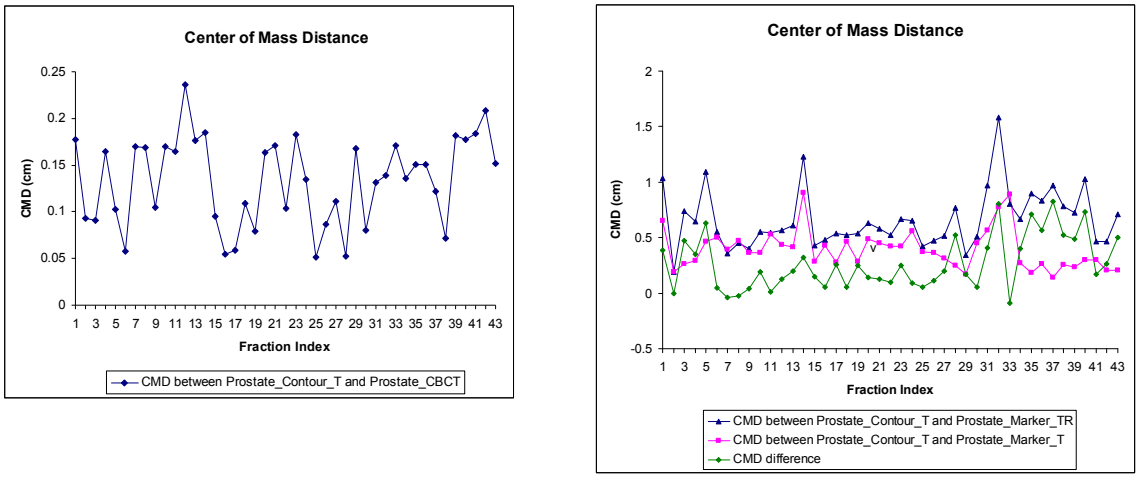

(a) (b)

Figure 3 (a) Difference in the center of mass between the prostate contour transferred after contour registration and the prostate manually contoured on CBCT. (b) The center of mass distance of the prostate after marker registration with (Marker_T) and without (Marker_TR) rotational compensation.

(b) Task 1 (5) Atlas-based auto-segmentation

As stated in task 1-5, we intended to develop model-based contouring models to facilitate efficient delineation of the bladder and rectum for each MV-CBCT. Last year, we reported that the atlas-based autom-segmentation tool achieved a modest success. The average overlap between the manually drawn and master atlas-based contours for the prostate, lymph nodes, and rectum were 60%, 51%, and 64%, respectively. For the purpose of re-planning or online adaptation, we further hypothesize that the patient-specific atlas-based segmentation tool can improve overlap indices between the manually drawn and automatic contours significantly when compared to the general patient based atlas method. Moreover, use of diagnostic imaging for imaging guidance will further improve performance of atlas-based auto-segmentation (ABAS).

From our registry of prostate cancer, we chose seven patients, who underwent external beam treatment of prostate cancer with daily diagnostic CT-in-room imaging guidance for 38 treatment sessions. For each patient, the prostate, rectum and bladder were manually contoured based on the protocol of Radiation Therapy Oncology Group (RTOG 0126). To test efficacy of the patient-specific atlas, three patient-specific atlases were created for each patient, consisting of one, four and seven prior contour and image sets. These atlases were then used to automatically generate contours for the last seven daily verification CT images of the patient. The automatically and manually generated contours were compared using the overlapping index (OI) and dice similarity coefficient (DSC). Statistical significance was assigned at $P<0.05$ for two-tail student *t* test.

As an example, Figure 4 compares the manual and automatic contours of the bladder, rectum, and prostate for a patient, using atlases comprised of 1, 4, 7 image sets. Among these patients, auto-contours of the bladder obtained from all atlases were highly consistent with the manual contours. The OI and DSC were above 96% and 91%, respectively. For the prostate, the OI and DSC for 7-

image set (87.8±5.4% & 86.6±4.9%) and 4-image set (88.8±4.0% & 87.1±3.2%) atlases were similar, both significantly higher than those from 1-image set atlas (84.6±5.5% & 82.5±6.4%). For the rectum, the OI and DSC topped at 86.2±9.2% and 87.8±9.9% for 7-image set atlas, followed by 82.8±14.6% and 84.7±8.8% for 4-image set atlas, and 80.9±13.1% and 80.9±8.8% for 1-image set atlas. The summary of these results are shown in Figure 5. The times for manual and automatic contouring were approximately 20 minutes and 1 minute, respectively. A manual 'fine tuning' of the auto-segmentation required about 6 minutes. With verification images having the same quality of the planning images, patient-specific atlas-based auto-segmentation can provide fast and consistent delineation for prostate cancer on a daily basis. The inclusion of more than four to seven CT sets in atlas further improves the contouring results.

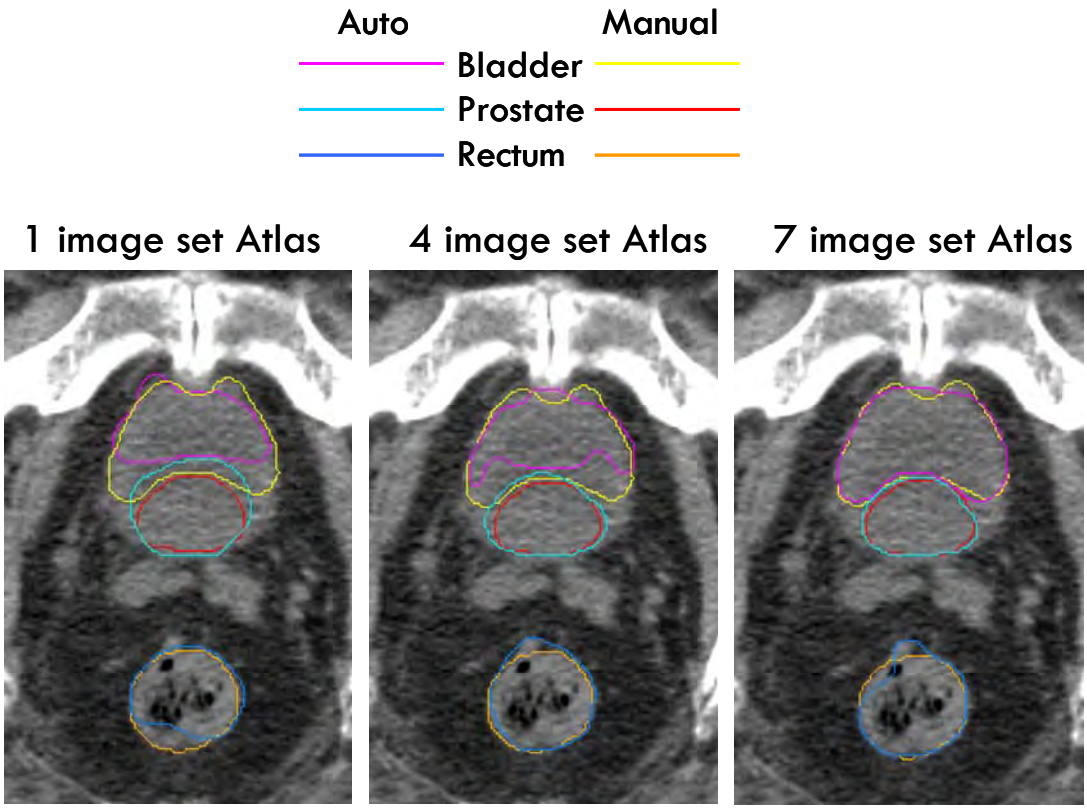

Figure. 4. Manually and automatically generated contours on a representative mid-level slice with prostate, bladder and rectum all presented.

Compared with non-patient-specific atlas, patient-specific atlas yielded significantly more accurate contours. Figure 6 compares the effect of patient-specific versus non-patient-specific atlas performances. For three structured contoured, both DSC and OI from patient-specific atlas were significantly better than those obtained with the non-patient-specific atlas. Rectum exhibited the greatest differences in output (>40 %) in response to this change of atlas components. The use of non-patient-specific atlas decreased the DSC and OI from over 80% to a low level of 50.2±13.5% and 46.8±12.9%, respectively.

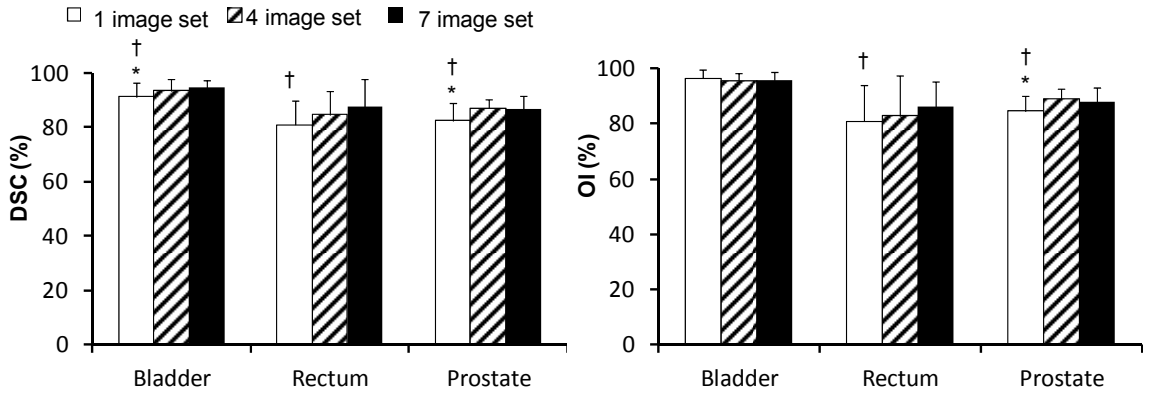

Figure 5. OI and DSC of different sized atlas for all ROIs. * P<0.05 between 1-image set and 4-image set atlases. †P<0.05 between 1-imaging set and 7-imaging set atlases. ‡ P<0.05 between 4-imaging set and 7-imaging set atlases.

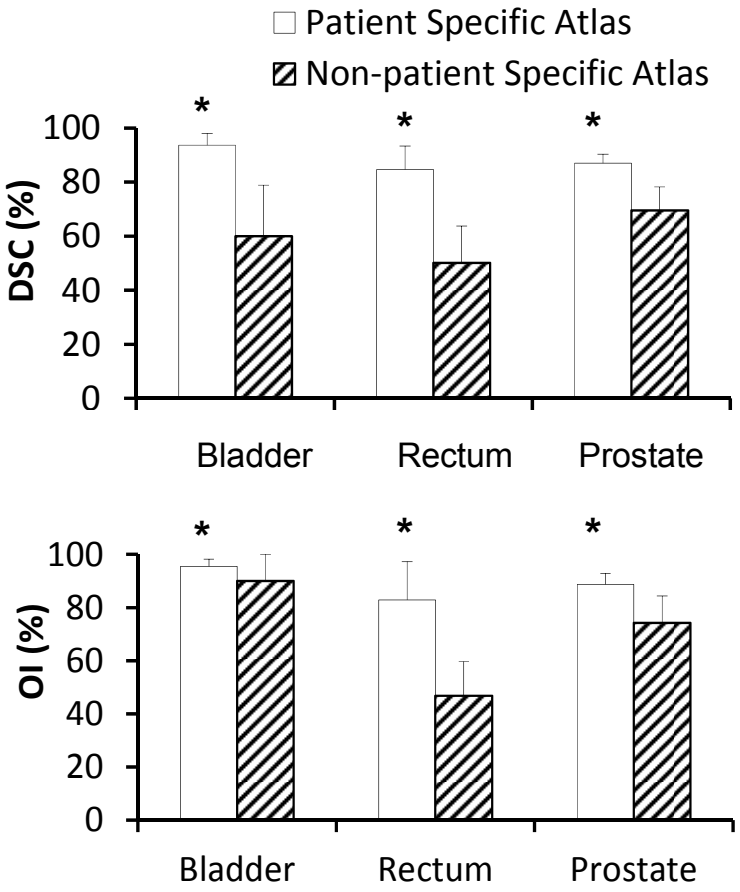

Figure 6. Effect of the use of patient specific atlas for ABAS. DSC and OI were generated with four-image set atlas. * P<0.05 compared to results obtained using non-patient specific atlas.

The reproducibility of atlas-based auto-segmentation performance was validated by the second observer as shown in Figure 7. The DSC and OI were similar with those obtained from the first observer for all three regions of interests, suggesting a strong reproducibility of the ABAS method. On the other hand, compared with the inter-observer variation in manual contours, ABAS yielded comparable geometrical similarity indices (< 3%) for both bladder and prostate. The ABAS generated indices (DSC: 81.0±6.7% and OI: 81.1±12.9%) were lower than the inter-observer variation (DSC: 87.5±4.5% and OI: 93.3±3.4%) for rectum because of the presence of air bubbles and large anatomical changes. These suggest that a manual 'fine tuning' process may significantly improve the contouring accuracy of rectum, while it is less critical for prostate and bladder.

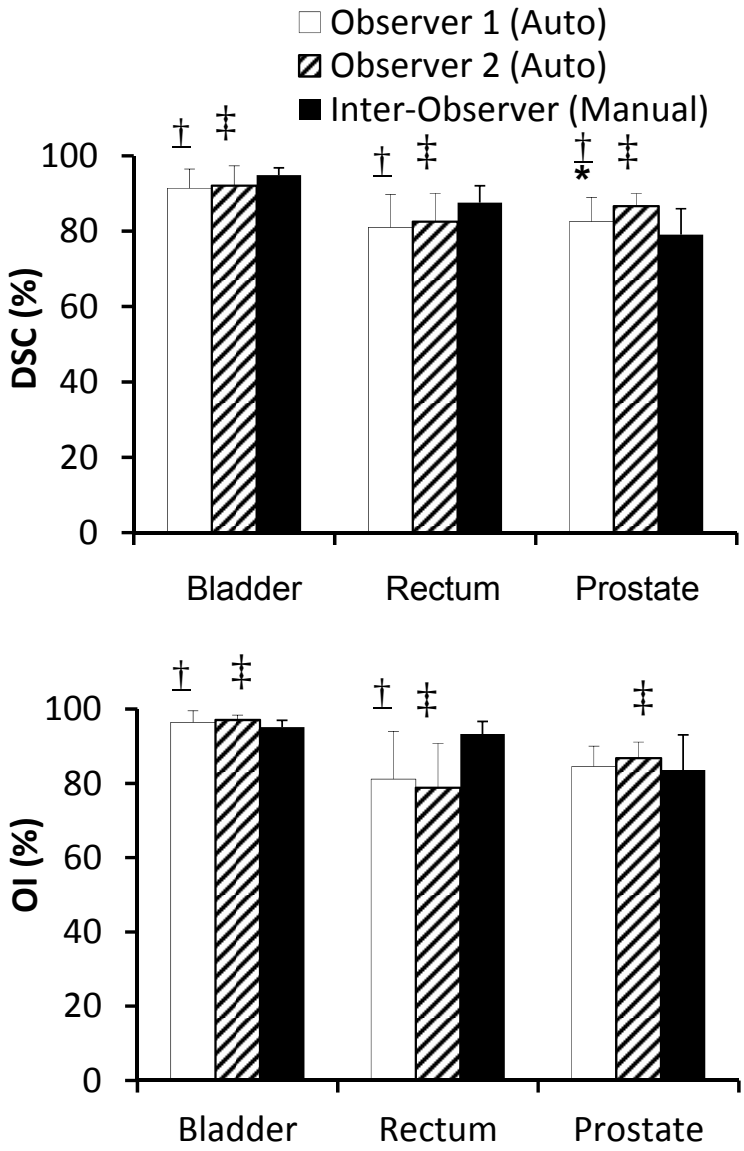

Figure 7. Reproducibility study of ABAS methods. ABAS was performed with single-image set patient specific atlas. DSC and OI were obtained on the same 21 image sets from two independent observers. *P<0.05 compared to ABAS results from the 2nd observer. †P<0.05 compared to the inter-observer variations for manual contours. ‡ P<0.05 compared to the inter-observer variations for manual contours.

In conclusion, the use of patient-specific atlas can produce automatic contours that were highly consistent with the manual ones. The inclusion of multi-image sets in the atlas further improves the performance. Since the use of diagnostic images for imaging guidance is not widely available clinically, we plan to validate our results with kilo-voltage cone beam CT, which is predominantly used for daily imaging guidance. Our results demonstrate the application potential of ABAS for adaptive planning to compensate independent inter-fractional organ motions in concurrently treatment of the prostate and pelvic lymph nodes. The completed manuscript is attached in appendix B.

(c) Task 1 (6) and Task 3 (4&5) Comparison of ideal MAP plans with MLC-MAP plans

To establish evaluation criteria for our proposed adaptive strategies, we need to create a set of IMRT plans, which retrospectively simulate on-line planning based on the acquired daily verification images. These sets of simulated on-line plans are referred to as ideal MAP plans. Because real-time planning is not yet clinically practical, we proposed an adaptive strategy by shifting multi-leaf collimator (MLC) leaves without requiring real-time planning or dose recalculation. The plans created with this method are referred to as MLC-MAP plans.

Six patients with a total 124 fractions of kV-CBCT images with concurrent prostate and lymph nodes treatment were consented for this retrospective study. For each KV-CBCT, the contours of prostate, bladder, and rectum were manually delineated. Assuming that the lymph nodes are fixed with respect to bony anatomy, the contours of lymph nodes were transferred from the planning CT after bone-based rigid image registration. The daily prostate displacements were obtained using dual image registrations: alignment to the bone and alignment to the prostate. For each fraction, four IMRT plans were created: (a) MLC-shifting plan; (b) iso-center shifting plan according to alignment to the bony structures; (c) iso-center shifting plan according alignment to the prostate contour of the day; (d) simulated real time plan. When comparing these four types of plans, we evaluated the dose to 95% (D95) of the prostate and lymph nodes, and dose to 5% and 50% (D5 and D50) of the rectum and bladder. These dosiemetric endpoints were efficiently extracted by another in-house program as described in Task 2 (item 2).

To create MLC-shifting plans, we used an in-house program to automatically shift each segment of the original IMRT plan. This in-house program was developed last year, as described in Task 2 (item 1), and the program automatically identified MLC pairs that were collimated to the prostate and adjusted the positions of those leaf pairs according to measured prostate displacements. The shifts MLC positions were then input back to the planning system and applied to the corresponding KV-CBCT for dose calculations.

To create iso-center shifting plan based on bony registration, we used the daily KV-CBCT as the primary images for dose calculation, then shifted the KV-CBCT acquisition center according to the shifts after bony registration, and set this shifted center as the treatment iso-center. Finally, we associated the input for each segment of the original IMRT plan with the new iso-center and performed dose calculation based on the KV-CBCT of the day. Following the same procedure, we created contour iso-center shift plans. In these plans, the iso-center of each daily KV-CBCT was shifted according to the alignment of the prostate contour of the KV-CBCT with the prostate contour of the planning CT.

For the ideal MAP plans, or simulated real-time plan, we set the iso-center as the iso-center in the bony iso-shifting plans and performed a full-fledged optimization to create simulated real-time plan. Because of unstable CT numbers in the KV-CBCT, we manually set

the physical density of the KV-CBCT to 1 for all plans based on KV-CBCT.

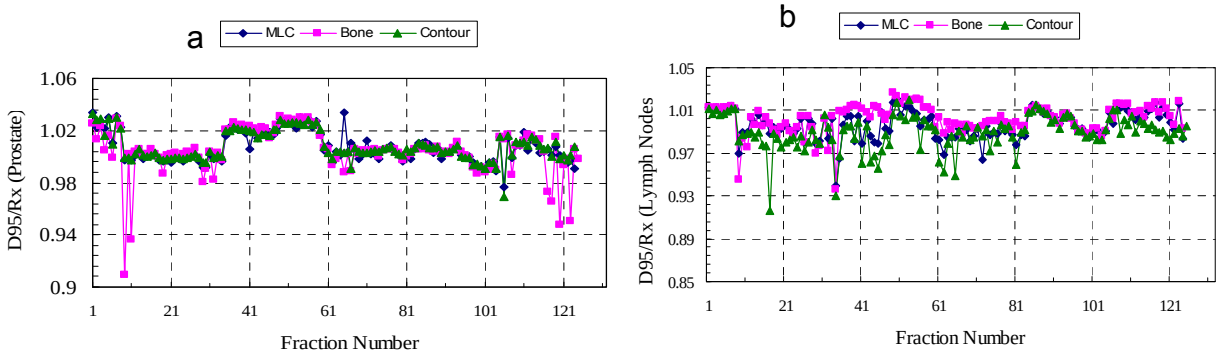

Figure 8. Normalized to the daily planned dose received by 95% (D95) of the prostate, daily dose of D95 of the prostate (in a) and D95 of the pelvic lymph nodes (in (b) calculated based on daily KV-CBCT for MLC-shift, bone iso-shift and contour iso-shift methods.

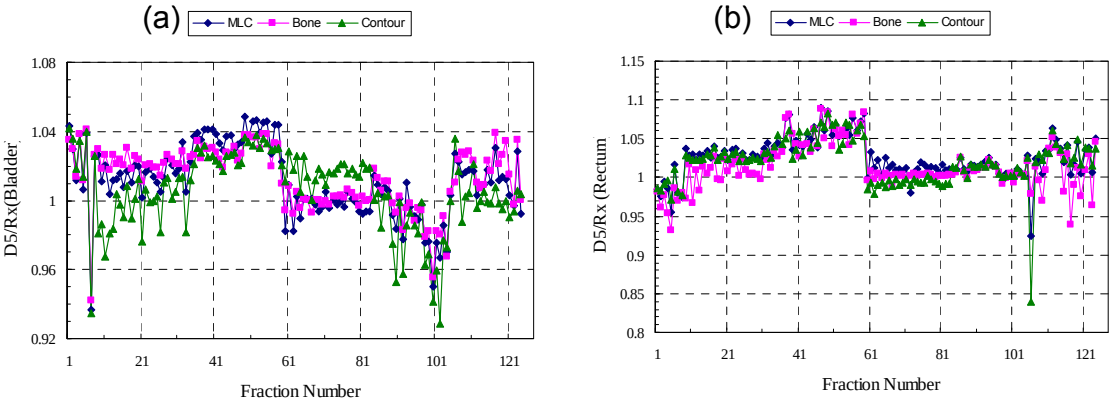

Figure 9. Normalized dose to the planned daily dose received by 5% (D5) of the bladder and rectum, respectively, (a) daily D5 of the bladder and (b) daily D5 of the rectum calculated based on daily KV-CBCT for MLC-shift, bone iso-shift and contour iso-shift methods.

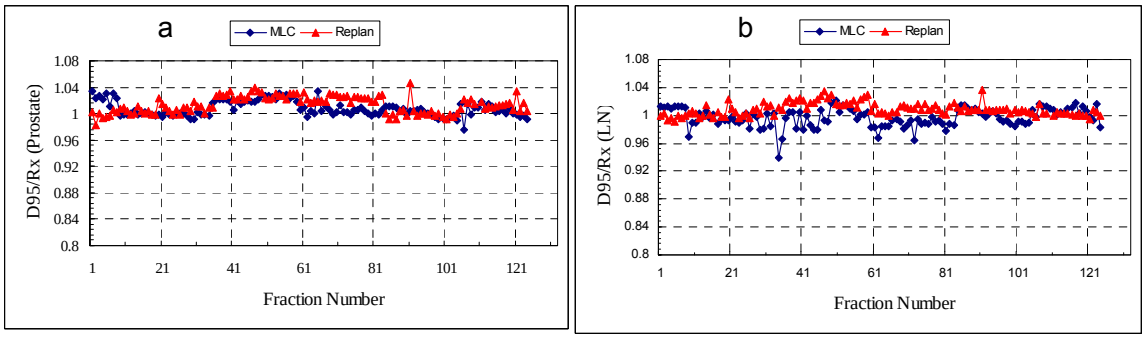

Figure 10. Normalized to planned daily dose to 95% (D95) of the prostate, daily D95 of the prostate (a) and D95 of the pelvic lymph nodes (b) calculated based on daily KV-CBCT for MLC-shifting and real time planning (re-plan) plans.

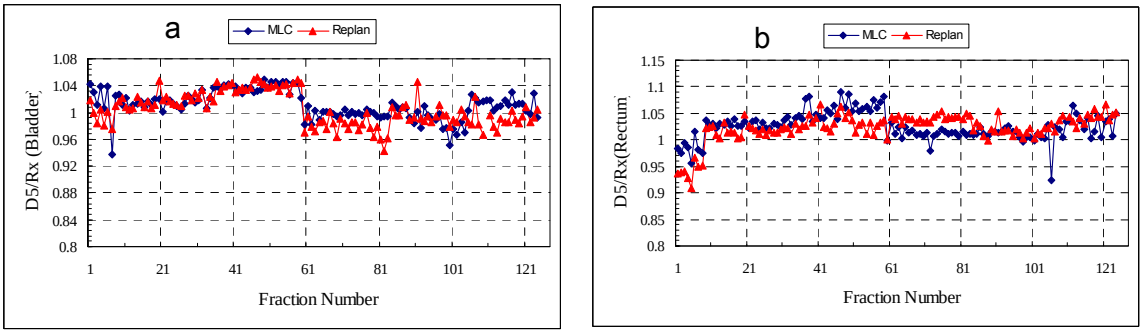

Figure 11. Normalized to the planned dose to 5% of the bladder (D5) and rectum (D5), daily dose to 5% (D5) of the bladder in (a) and rectum in (b) calculated based on daily KV-CBCT for MLC-shifting and real time planning (re-plan) plans.

From Figures 8-11, we found that the MLC-MAP method can achieve that daily dose to 95% of prostate and lymph nodal volumes were > 97% of the planned daily dose (referred to as Rx dose), compared to > 92% of the planned daily dose for the conventional iso-center shift methods. When compared to the real-time planning method, MLC-shifting plans achieved similar dose coverage to the prostate. For the pelvic lymph nodes, except for a few fractions, the dose coverage was adequate. Moreover, the MLC-shifting plans did not increase dose to the sensitive structures such as the bladder and rectum.

Key Research Accomplishments

(a) We found that the rotation detected by registering implanted markers may not reflect true rotation of the prostate. Ignoring these detected rotations may lead to erroneous errors of determining the true prostate potion.

(b) We found that compensating for the prostate rotations detected based on marker registration can be compensated with translational shifts. Such compensation will significantly improve geometric and dosimetric indices.

(c) We found that when the verification images had the same quality of planning CT, the use of patient-specific atlas could produce automatic contours that were highly consistent with the manual contoured ones.

(d) Performance of patient-specific atlas is drastically better than general patient population-based atlas.

(e) The inclusion of multi-image sets (four or more) in the patient-specific atlas can further improve the performance.

(f) We found that iso-center shifting based on the bony alignment plans achieved adequate dose coverage for the pelvic lymph nodes, but not sufficient for the prostate. In contrary, the iso-center shifting based on the prostate contour alignment plans achieved adequate dose coverage for the prostate, but not sufficient for the pelvic lymph nodes. MLC-shifting plans provide the best compromised solution.

(g) When compared to the ideal plan with real-time planning, the MLC-shifting plans achieved similar dose coverage for the prostate. Except for a few fractions, MLC-shifting plans also achieved similar dose coverage for the pelvic lymph nodes. For the bladder and rectum, the MLC-shifting plans achieved comparable endpoint doses as the ideal plans.

Reportable Outcomes

(a) Qingyang Shang, Lawrence Sheplan, Kevin Stephans, Rahul Tendulkar, and Ping Xia: " Daily Prostate Rotation should be Compensated in Translational Correction and not to be Ignored", abstract, poster presentation at the Annual Meeting of American Association of Physicists in Medicine at Vancouver, BC, Canada, July 31-August 4, 2011 (Appendix D).

(b) Guangshun Huang, Naichang Yu, Kevin Stephans, Rahul Tendulkar, and Ping Xia: "Assessing Planning Margins Using Shifting Dose Matrix Method to Calculate Daily and Cumulative Doses Under Imaging Guided Radiotherapy (IGRT)." abstract, poster presentation at the Annual Meeting of American Association of Physicists in Medicine at Vancouver, BC, Canada, July 31-August 4, 2011 (Appendix E).

Conclusion

In summary, in this period of research we completed a manuscript for which the abstract was reported in last year's report (in Appendix C). We investigated the possibility of a large rotational shift that was detected based on marker-based image registration by selecting patients with three implanted markers and with kilo-voltage cone beam CTs. We found that most detected rotational shifts can be compensated by translational shifts, and ignoring these rotational shifts may lead to erroneous prostate positioning resulting in missing the radiation target of the prostate. Using general patient population-based atlas, our results last year showed a modest performance. This year, we used diagnostic quality verification images to construct patient-

specific atlases, and we found that the patient-specific atlas can produce automatic contours that were highly consistent with the manually contoured ones. We plan to validate this finding by using kilo-voltage cone beam CTs next year, since kilo-voltage cone beam CTs are widely used as verification images clinically. When compared to the ideal MAP plans, we found that MLC-shifting plans achieved comparable dose coverage to the prostate and, with the exception of a few fractions, MLC shifting plans were also comparable to the ideal MAP plans for the pelvic lymph nodes. We speculated that in these few exceptional fractions, a finer MLC leave width (<0.5 cm) may improve the result, or using a combination of treatment table movement and MLC shifting may improve the outcomes. Furthermore, our dosimetric evaluation is mostly based on daily doses. We plan to examine dosimetric effect from a total delivery dose by accumulating daily dose from the verification CTs.

Appendices

Appendix A:

Daily Prostate Rotation Can Be Compensated in Translational Correction

Qingyang Shang, Lawrence J. Sheplan Olsen, Kevin Stephans, Rahul Tendulkar, and Ping Xia

Department of Radiation Oncology, Cleveland Clinic, Cleveland, Ohio 44195

Abstract

Daily prostate displacement can be determined by registering the implanted fiducial markers from the planning CT with the daily verification images. However, the detected rotational shifts may not be corrected due to practical reasons. The question is what the dosimetric impact is if the rotational shifts are not corrected and what the dosimetric gain is if the rotations are compensated with translational shifts. The aim of the study is to quantify geometric and dosimetric effects of rotational shifts with and without corrections. Five patients, with 43 kilo-voltage cone beam CT (KV-CBCT) and implanted markers, were selected for this retrospective study. The prostate, bladder, and rectum were manually contoured on each CBCT by a physician. Two methods were applied to register markers from CBCTs with those from the planning CT: one method allowed both translational and rotational shifts to align the markers first and then zero out the rotation, mimicking the frequent clinical practice in situations without a six-degree treatment table; the other method allowed only translational shifts to align markers, partially compensating the prostate rotations by translational shifts. Center of mass distance (CMD) and Overlap index (OI) were evaluated as geometric indices for these two registration methods. Their dosimetric effects were also analyzed by comparing the dose coverage of the prostate clinical target volume (CTV) and the possible reduction of the planning margin. We found that prostate rotational shifts dominated in the left-right axis, with respective systematic and random

components of 4.6° and 4.1°. When the rotational shifts were greater than 10°, the differences in CMD between the two marker registrations were greater than 5 mm in 85.7% of these fractions; when the rotational shifts were greater than 6°, the differences of CMD were greater than 4 mm in 61.1% of these fractions. The analysis of OI showed that, to achieve 95% overlap between the “prostate at planning” and the “prostate of the day”, a planning margin reduction of 2mm in 3 out of 5 patients (66.7%) was achieved when marker registration with translational compensation was used. Dosimetrically, with 2 mm margin reduction, the average daily dose to 95% of the prostate (D95) were 1.97 Gy and 1.91 Gy for the methods with and without compensation, respectively ($p = 0.03$). In conclusion, compensating for the rotations with translational shifts can improve geometric and dosimetric indices when a six-degree couch is not available.

1. Introduction

External beam radiation therapy is one of the most commonly used techniques for prostate cancer treatment. During the course of the treatment, which takes typically several weeks to complete with daily treatment delivery, the prostate moves frequently and randomly relative to the pelvic bones because of the variable filling and emptying of the bladder and rectum (Langen and Jones, 2001; Byrne, 2005). Such geometric uncertainties pose a great challenge to precise prostate localization for treatment delivery. The use of image-guided radiotherapy (IGRT) improves treatment accuracy considerably by measuring patient setup error and internal organ motion, and incorporating the shift information into the correction strategies of the treatment plan. This technique allows effective reduction of clinical target volume (CTV) to planning target volume (PTV) margins, and thus improves normal tissue protection.

Using implanted markers as a surrogate to localize the prostate is a well-adopted method of daily IGRT (Khosa *et al.*, 2010). Because of their high contrast, the implanted markers can be easily detected by all common forms of X-ray imaging modalities, including conventional electronic portal images (EPI), stereoscopic kilo-voltage (KV)-images, mega-voltage cone beam computed tomography (MV-CBCT), kilo-voltage cone beam CT (KV-CBCT), and diagnostic CT-in-room. Alternatively, without the use of X-rays, implanted electromagnetic transponders (the Calypso system, Calypso Medical, Seattle, WA) can not only localize the prostate prior to treatment but also track the prostate motion during treatment. More importantly, registering three markers from the planning CT with the verification images can have an analytical solution, and thus the six degrees of shifts, including three translational and three rotational shifts, can be determined automatically.

Many studies investigated the rotational setup errors and rotational shifts of the prostate during the course of the treatment. Some studies have found that rotational setup errors are relatively

small (Guckenberger *et al.*, 2006; Remeijer et al., 2000), and that a robotic treatment couch could reduce the systematic component of the error (Soete *et al.*, 2006). In addition, studies have shown that the dosimetric effects of rotational setup errors are modest (Cranmer-Sargison et al., 2008)(Fu et al., 2006). Other studies, however, reported that the rotational errors of the internal organ are greater in magnitude and play a more important role in dosimetric impact than setup errors, so the rotational errors of the prostate have been the focus of more comprehensive studies (van Herk *et al.*, 1995; Stroom *et al.*, 1999; Dehnad *et al.*, 2003; Aubry *et al.*, 2004; Hoogeman *et al.*, 2005; Owen *et al.*, 2011; Wu *et al.*, 2006). To correct the rotational shifts of the prostate, several strategies have been proposed, such as online corrections by couch rotations (van Herten *et al.*, 2008), gantry and collimator angle adjustments to correct for left-right rotations (Rijkhorst *et al.*, 2007), and a hybrid approach of combining offline adaptive planning and online image guidance (Lei and Wu, 2010; Liu and Wu, 2011).

The calculated rotational shifts, however, may not be corrected due to several practical reasons, among which the most notable ones are: (a) a six-degree treatment couch is not available; (b) it may be unsafe to position a patient with large rotations. The question is: if the rotational shifts cannot be corrected, should they be compensated with translational shifts, or simply ignored? The purpose of this study is to investigate whether the rotational displacements of the prostate can be compensated with translational shifts and to quantify geometric and dosimetric effects with and without compensation.

2. Methods and materials

2.1. Patient selection and treatment planning

Five patients, who underwent definitive external beam radiotherapy, had three electromagnetic transponders implanted for daily IGRT using the Calypso 4D localization system (Calypso Medical, Seattle, WA). In addition, weekly or daily kilo-voltage cone beam CTs (KV-CBCT)

were also acquired to cross check the Calypso system, upon the request of radiation oncologists. A total of 43 KV-CBCTs were available for this retrospective study.

The patients were treated with two different dose schemes: 2 Gy per fraction to a total dose of 78 Gy; and 2.5 Gy per fraction to a total dose of 70 Gy. For the purpose of this study, the prescription of all plans was re-normalized to 2 Gy per fraction to a total dose of 78 Gy, without altering IMRT optimization. The CTV was the prostate, and the organs at risk (OAR) included the bladder and rectum. The planning margins for these patients were 4 mm posteriorly and 6 mm elsewhere. The IMRT plans were created with the Pinnacle treatment planning system (Pinnacle^3, Philips Radiation Oncology System, Madison, WI), using a typical five beam arrangement with 10 MV photon beams.

2.2. Quantification of the prostate displacement

On each KV-CBCT, the prostate, rectum, and bladder were manually contoured by a physician. Subsequently, each CBCT was registered with the corresponding planning CT using four different image registration methods (a total of 172 imaging registrations). The image registration methods used were: (a) manually align the bones with translational shifts only (Bone_T); (b) automatically align the three markers with both translational and rotational shifts (Marker_TR); (c) manually align the three markers with translational shifts only (Marker_T); and (d) manually align the prostate contour with translational shifts only (Contour_T). After subtracting translational shifts from the bony alignment (the first registration method), patient setup error was removed from the other three methods, defining the translational shifts of the prostate related to the pelvic bones. The prostate rotations from the second method were recorded. To investigate whether the rotational displacement of the prostate can be compensated with translational shifts, we used the contour registration method (Contour_T) as a benchmark to evaluate the two marker registration methods (Marker_TR and Marker_T) by comparing their geometric and dosimetric indices.

2.3. Geometric analysis

Because of limited soft tissue contrast in each KV-CBCT, prostate contours manually drawn on the KV-CBCTs may be subject to some uncertainties and variations. To minimize these variations, for the marker based alignments, the prostate contours were transferred from the planning CT after registration. To avoid unnecessary variables in comparison of geometric and later dosimetric parameters for the registration methods investigated in this study, we used all transferred contours from the planning CT, including the contour based registration method. Thus, for each patient, after applying each method of registration, the planning prostate contour was transferred from the planning CT to the registered CBCT. The transferred planning contours, denoted as Prostate_Marker_TR, and Prostate_Marker_T, and Prostate_Contour_T, corresponded to the Marker_TR, Marker_T, and Contour_T registrations. All these contours were CTV contours. For the Marker_TR registration, rotations were ignored for contour transferring, reflecting clinical practice without a six-degree treatment couch. The manually drawn prostate contour on the CBCT was denoted as Prostate_CBCT. FIG. 1 is an example illustrating these prostate contours obtained from different registration methods.

2.3.1. Center of mass distance

For each of these prostate contours, a center of mass (COM) was calculated in the same CBCT frame. As a global measure of daily prostate displacement, the Center of Mass Distance (CMD) of the prostate contours between the bony registration and each of the other three registration methods was calculated using the following equation:

$$d = \sqrt{(x - x_0)^2 + (y - y_0)^2 + (z - z_0)^2} \tag{1}$$

where d is the CMD, and x, y and z are the coordinates of the COM of the transferred prostate contour after each registration method, and x_0, y_0 and z_0 are the coordinates of the COM of the transferred prostate contour after bony registration. Using this equation, we verified the result of

the contour based registration by calculating the relative CMD between the Prostate_CBCT and the Prostate_Contour_T.

Using the contour registration (Contour_T) as a benchmark, we compared the accuracy of the two marker registration methods (Marker_TR and Marker_T) by calculating the relative CMDs between the Prostate_Contour_T and Prostate_Marker_TR, and between the Prostate_Contour_T and Prostate_Marker_T.

2.3.2. Overlap index

To quantitatively evaluate the geometric properties of the two marker registration methods, we defined the volume overlap index (OI) as

$$OI = \frac{Prostate\_Contour\_T \cap T[Prostate\_CT]}{Prostate\_Contour\_T} \tag{2}$$

where T is the transformation applied to the prostate contour from the planning CT (Prostate_CT) by the two marker registration methods, and the operator $\cap$ defines the common area between the two regions of interest. Thus we have

$$OI_{TR} = \frac{Prostate\_Contour\_T \cap Prostate\_Marker\_TR}{Prostate\_Contour\_T} \tag{3}$$

and

$$OI_{T} = \frac{Prostate\_Contour\_T \cap Prostate\_Marker\_T}{Prostate\_Contour\_T} \tag{4}$$

where subscript TR and T represent the Marker_TR and Marker_T methods, respectively. It should be noted that the OI increases as the CTV to PTV margin of the Prostate_Marker_TR or Prostate_Marker_T contour increases. We further computed and compared OI_{TR} and OI_{T} with different margins (0 mm, 2 mm, 4 mm, 6 mm and 8 mm) for each patient.

2.4. Dosimetric analysis

Dosimetric effect can be influenced by the initial planning margin, which was 4 mm posterior and 6 mm elsewhere. Instead of re-planning using progressively reduced planning margins, which may introduce variations in plan quality, we created new expanded CTVs to evaluate dosimetric effect if the IMRT plan were re-planned with reduced margins. Four new CTVs were created by three dimensionally expanding the Prostate_CBCT contour with 2 mm, 4 mm, 6 mm, and 4 mm posterior and 6 mm elsewhere (denoted as 6/4 mm). We calculated the dose to 95% of the volume of these newly defined CTVs (D95), and the dose to 5% and 50% of the volume of the bladder and rectum (D5 and D50). In such an approach, we examined the possible reduction of CTV to PTV margin for each marker registration method.

To calculate the dose at each fraction for each patient, the treatment isocenter was adjusted according to the computed shifts from the three registration methods, Marker_TR, Marker_T, and Contour_T.

3. Results

3.1. Prostate rotational shifts

Rotational shifts of the prostate detected from the Marker_TR registration were recorded and shown in FIG. 2 (a) for all 43 fractions. The rotational shifts around anterior-posterior (AP) and superior-inferior (SI) axes were relatively small and primarily within the range of -5° and +5°, while the shifts around left-right (LR) axis had larger magnitude and it exceeded 10° at times. The overall mean and standard deviation (SD) of the rotational shifts about the three axes were 3.3±5.8°, -1.4±2.9°, and -0.8±2.8°, for the LR, AP and SI axes, respectively. The systematic and random SDs are listed in Table I. FIG. 2 (b) shows the distribution of the prostate rotations around the LR, AP and SI axes. Again, rotations around the LR axis had a boarder distribution than the rotations about the other two axes, and they also presented extreme values (> 10°).

3.2. Geometric analysis

The CMD between the transferred prostate contour based on contour registration and the physician drawn contour on the CBCT is shown in FIG. 3(a). Such distance was detected to be less than 1.9 mm (1.3 ± 0.5 mm) for 95.3% of all treatment fractions, with exception of two fractions with a distance of 2.1 and 2.4 mm, respectively.

FIG. 3(b) demonstrates the CMDs between the Contour_T shifted and the Marker_TR or Marker_T shifted prostate, and the difference between the two. It shows that the Prostate_Marker_T is closer to the Prostate_Contour_T than the Prostate_Marker_TR, especially when the rotation is large. The difference between the two CMDs ranged from -0.9 to 8.3 mm when the maximum rotation (absolute value) from all three axes varies from 0.9° to 13.8°. The mean CMDs between the Prostate_Contour_T and Prostate_Marker_TR or Prostate_Marker_T were 6.6 and 4.0 mm, respectively. When the rotation was greater than 10°, the difference in CMD between the Marker_TR and Marker_T registrations was greater than 5 mm in 6 out of 7 (85.7%) of such fractions. When the rotation was greater than 6°, the difference in CMD was greater than 4 mm in 11 out of 18 (61.1%) cases. The statistics of the two CMDs and their difference are summarized in Table II.

FIG. 4 compares the average OI for the Marker_TR and Marker_T methods from 5 fractions for one patient as a function of the CTV-PTV margin. In general, OI_T is greater than OI_{TR}, and as the margin increases, both OIs approach to 1. For this patient, to achieve 95% overlap between the “prostate of the day” and the “prostate at planning”, 6 mm margin was required for the Marker_TR method, while only 2 mm was necessary for the Marker_T method.

3.3. Dosimetric analysis

To illustrate the dosimetric effect of the two marker registration methods, D95 of the original and expanded prostate CTVs were computed and compared. FIG. 5 shows the mean and standard deviation of the daily CTV D95 versus CTV expansion margins for the three registration methods. It is noted that for the original CTV, the dose coverage does not present a significant difference between the two marker registrations ($p = 0.87$) from the paired Student's t-test; however, for the four new expanded CTVs, D95 of the Marker_TR are significantly lower compared with the Marker_T method ($p < 0.05$). For example, with 2 mm margin reduction (corresponding to 2 mm CTV expansion in this study), the average daily D95 were 1.91, 1.97 and 2.01 Gy for the Marker_TR, Marker_T and Contour_T methods, respectively ($p = 0.03$).

FIG. 6 plots the percentage fractions in which the CTV D95 is less than 95% (FIG 6 (a)) and 99% (FIG 6 (b)) of the prescribed dose as a function of the CTV expansion margins. For example, when CTV was expanded with 2 mm margin, 27.9% fractions had D95 less than 95% of the prescription dose for the Marker_TR method, compared with 11.6% for the Marker_T method. Furthermore, when 99% of the prescribed dose was required, 44.2% fractions failed this criterion for the Marker_TR, in contrast to 20.9% for the Marker_T. The detailed statistics of D95 below 95% and 99% are listed in Table III.

FIG. 7 shows the daily D5 and D50 for the bladder and rectum, together with the p-value for the two marker registration methods. The doses to bladder and rectum did not reach statistically significant difference (p-value for D5, D50 of the bladder, and D50 of the rectum were 0.15, 0.41 and 0.55, respectively) by the Marker_TR and Marker_T methods, except for the case of D5 for the rectum ($p = 0.02$).

4. Discussion

In this work, we investigated the magnitude and distribution of the prostate rotational shifts, and evaluated the geometric and dosimetric effects of the rotations on the treatment plan for prostate

cancer. It is difficult to deal with rotational setup error and prostate rotational displacement concurrently, because rotation is not a variable that can be manipulated in the same way as translation, even if it can be measured. Thus in bony registration, we aligned the two images with translational only shifts, implicitly including rotational setup error through translational compensation. Since the rotational setup errors are usually small, this compensation is trivial too. We focused our study on the more significant translational compensation for internal prostate organ rotations.

Systematic and random components of interfraction rotations of the prostate are two important measures to evaluate the organ motion. Expressed as a standard deviation (SD), the systematic component describes the variation of the mean displacement of the prostate, while the random component delineates the day-to-day variation. Our data for both systematic and random components of prostate rotation, together with those reported in the literature, are shown in Table IV. Because of the difference in treatment protocols, image registration approaches, and mathematical methods used for error computation in each institution, discrepancy is observed in these results. Some studies (van Herk *et al.*, 1995; Stroom *et al.*, 1999; Hoogeman *et al.*, 2005) matched the prostate contours in the planning CT with those in the repeated CT scans to get the rotational shifts of the prostate relative to the pelvic bones, while others (Dehnad *et al.*, 2003; Aubry *et al.*, 2004; Owen *et al.*, 2011), similar to what we did in this study, performed the registration based on the implanted markers. From Table IV, it is observed that all contour registrations (the first three methods) tends to have a smaller rotation around AP axis for both systematic and random variations, compared with marker registrations. In addition, the mathematical equations used to compute the systematic and random errors might be slightly different from one study to another. For example, Owen et al. computed the errors using the method described by van Herk (van Herk, 2004); Stroomet al. and Hoogeman et al. utilized similar method but corrected the systematic error for the finite number of measurements; Aubry

et al. and we employed an approach by Remeijer et al. (Remeijer *et al.*, 2000), not only considering the limited size of samples, but also accounted for the different number of measurements for each patient. Furthermore, Owen et al. used the marker placed near the apex of the prostate as the pivot point for rotation computation, while for all the other studies, including ours, rotations were measured at the center of mass of the prostate contour or markers. Despite these differences, prostate rotation around LR axis was found to be greater than that of the other two axes (except for the study conducted by Owen et al.).

In this study, we assumed the prostate be a rigid body in order to focus on the analysis of the rotational shifts of the organ. The actual shape of the prostate may vary from day to day. Furthermore, due to uncertainties in contouring the prostate on CBCT images, there was discrepancy in the CMD between the prostate contour from contour registration and the daily prostate contour on CBCT, however it remained within 2 mm. Both CMD and OI analyses show that, geometrically, the Marker_T registration brings "prostate at planning" closer to "prostate of the day", thus provides more accurate prostate localization. OI_T demonstrates higher value than OI_{TR}, indicating that with the same CTV to PTV margin, the Marker_T registration leads to better dose coverage than the Marker_TR. Alternatively, to achieve similar dose coverage, the Marker_T registration requires smaller planning margins than the Marker_TR. For example, if 95% overlap is required, compared with the Marker_TR, the Marker_T method requires a smaller margin in 4 out of 5 patients, of which 3 cases have a margin reduction over 3 mm. Unlike CMD, OI is a volumetric measure of the proximity between the marker shifted prostate contour (Prostate_Marker_TR or Prostate_Marker_T) and contour shifted prostate (Prostate_Contour_T). It regards the prostate gland as a 3D volume rather than a single point (as in the CMD analysis). Thus, as a quantitative evaluation of the accuracy of the registration methods used for prostate localization, OI incorporates more spatial information into the analysis, and consequently, it is less sensitive to the uncertainties than the CMD analysis.

Geometrically, the Marker_TR method offers an inferior overlap between the “prostate at planning” and the “prostate of the day” to the Marker_T; but dosimetrically, it provides similar acceptable dose coverage to the prostate as the latter one does ($p = 0.87$). A reasonable explanation could be that, for the patients available in this study, the CTV to PTV margin of the plan is generous enough to enclose any shifts caused by prostate rotations. The current trend in many clinical settings is an attempt to reduce planning margins in order to spare more surrounding normal tissue, while maintaining similar effectiveness to prior techniques. Our study shows that if the planning margin were to be further reduced, the method of compensation rotation with translational corrections will begin to play a bigger role in the daily patient setup, and the Marker_T method will outperform Marker_TR substantially.

This hypothesis was confirmed by the dosimetric analysis of the D95 for the expanded prostate CTV. Instead of performing re-planning with various margins for each patient, we expanded the prostate CTV with margins of 2 mm, 4 mm, 6/4 mm, and 6 mm, resulting 4 plans with reduced planning margins (4/2, 2/0, 0, and 0/-2). D95 of the Marker_T is superior to that of the Marker_TR as the equivalent planning margin decreases, indicating that when the CTV to PTV margin is reduced (compared with the original plan), the Marker_T method provides better dose coverage for the CTV ($p < 0.05$). Thus the same conclusion can be drawn as the geometric analysis. As for the critical structures, these two marker registration methods do not significantly affect doses to the bladder ($p > 0.05$). For the rectum, D50 of the Marker_TR method is not statistically different from that of the Marker_T ($p > 0.05$), but the former method showed a lower D5 value ($p < 0.05$). A further investigation revealed that for one patient, the Marker_TR method shifted the prostate contour anteriorly, away from the rectum, causing less dose received by the rectum D5, which is a more sensitive measure than D50. However, the CTV in these fractions also received inadequate dose. Thus, a lower D5 for rectum does not imply that the Marker_TR is a better solution.

In summary, the Marker_TR and Marker_T registration methods were compared in this study. The former method ignores rotational shifts of the prostate detected by the implanted fiducial markers, imitating current clinical practice when a six-degree treatment table is not available; and the latter one uses only translational shifts to interpret prostate motion, compensating the shifts caused by rotation through translation only registration. Geometric and dosimetric evaluations of the two methods suggested that the Marker_T method is an effective strategy for prostate rotation compensation. Current planning margin may be larger than necessary if correcting for rotational shifts in all three axes, but as margins are decreased, dosimetric coverage may be significantly inferior (and clinically unacceptable) with the marker registration method with the rotational shifts ignored when compared to the other techniques.

5. Conclusion

This study indicated that the rotational shift of the prostate resulted from marker registration may be non-negligible. Without a six-degree table, prostate rotations are often not corrected. Simply ignoring large rotations may lead to increased planning margins or diminished dose coverage. Compensating for the rotations with translational shifts is effective and superior to ignoring rotations, achieving better tumor coverage without significantly affecting surrounding OARs.

Acknowledgements

This research is supported in part by the United States Army Medical Research and Material Command (USAMRMC, PC073349).

References

Aubry J F, Beaulieu L, Girouard L M, Aubin S, Tremblay D, Laverdiere J and Vigneault E 2004 Measurements of intrafraction motion and interfraction and intrafraction rotation of prostate by three-dimensional analysis of daily portal imaging with radiopaque markers *Int J Radiat Oncol* 60 30-9

Byrne T E 2005 A review of prostate motion with considerations for the treatment of prostate cancer *Med Dosim* 30 155-61

Cranmer-Sargison G 2008 A treatment planning investigation into the dosimetric effects of systematic prostate patient rotational set-up errors *Medical Dosimetry* 33 199-205

Dehnad H, Nederveen A J, van der Heide U A, van Moorselaar R J A, Hofman P and Lagendijk J J W 2003 Clinical feasibility study for the use of implanted gold seeds in the prostate as reliable positioning markers during megavoltage irradiation *Radiotherapy and Oncology* 67 295-302

Fu W, Yang Y, Li X, Heron D, Huq M and Yue N 2006 Dosimetric effect of patient rotational setup errors on prostate IMRT plans *Medical Physics* 33 2091-

Guckenberger M, Meyer J, Vordermark D, Baier K, Wilbert J and Flentje M 2006 Magnitude and clinical relevance of translational and rotational patient setup errors: A cone-beam CT study *Int J Radiat Oncol* 65 934-42

Hoogeman M S, van Herk M, de Bois J and Lebesque J V 2005 Strategies to reduce the systematic error due to tumor and rectum motion in radiotherapy of prostate cancer *Radiother Oncol* 74 177-85

Khosa R, Nangia S, Chufal K S, Ghosh D, Kaul R and Sharma L 2010 Daily online localization using implanted fiducial markers and its impact on planning target volume for carcinoma prostate *J Cancer Res Ther* 6 172-8

Langen K M and Jones D T 2001 Organ motion and its management *Int J Radiat Oncol Biol Phys* 50 265-78

Lei Y and Wu Q W 2010 A hybrid strategy of offline adaptive planning and online image guidance for prostate cancer radiotherapy *Physics in Medicine and Biology* 55 2221-34

Liu H and Wu Q W 2011 Dosimetric and geometric evaluation of a hybrid strategy of offline adaptive planning and online image guidance for prostate cancer radiotherapy *Physics in Medicine and Biology* 56 5045-62

Owen R, Kron T, Foroudi F, Milner A, Cox J and Duchesne G 2011 Interfraction Prostate Rotation Determined from in-Room Computerized Tomography Images *Medical Dosimetry* 36 188-94

Remeijer P, Geerlof E, Ploeger L, Gilhuijs K, van Herk M and Lebesque J V 2000 3-D portal image analysis in clinical practice: An evaluation of 2-D and 3-D analysis techniques as applied to 30 prostate cancer patients *Int J Radiat Oncol* 46 1281-90

Rijkhorst E J, Van Herk M, Lebesque J V and Sonke J J 2007 Strategy for online correction of rotational organ motion for intensity-modulated radiotherapy of prostate cancer *Int J Radiat Oncol* 69 1608-17

Soete G, Verellen D, Tournel K and Storme G 2006 Setup accuracy of stereoscopic X-ray positioning with automated correction for rotational errors in patients treated with conformal arc radiotherapy for prostate cancer *Radiotherapy and Oncology* 80 371-3

Stroom J C, Koper P C, Korevaar G A, van Os M, Janssen M, de Boer H C, Levendag P C and Heijmen B J 1999 Internal organ motion in prostate cancer patients treated in prone and supine treatment position *Radiother Oncol* 51 237-48

van Herk M 2004 Errors and margins in radiotherapy *Semin Radiat Oncol* 14 52-64

van Herk M, Bruce A, Kroes A P, Shouman T, Touw A and Lebesque J V 1995 Quantification of organ motion during conformal radiotherapy of the prostate by three dimensional image registration *Int J Radiat Oncol Biol Phys* 33 1311-20

van Herten Y R J, de Kamer J B V, van Wieringen N, Pieters B R and Bel A 2008 Dosimetric evaluation of prostate rotations and their correction by couch rotations *Radiotherapy and Oncology* 88 156-62

Wu Q W, Ivaldi G, Liang J, Lockman D, Yan D and Martinez A 2006 Geometric and dosimetric evaluations of an online image-guidance strategy for 3D-CRT of prostate cancer *Int J Radiat Oncol* 64 1596-609

Table I. Prostate rotational shift variations in degrees.

	LR	AP	SI
Overall mean	3.3	-1.4	-0.8
Overall SD	5.8	2.9	2.8
Systematic SD	4.6	2.3	2.1
Random SD	4.1	2.0	2.0

Table II. Analysis of CMD of prostate shifts.

	CMD between Marker_TR and Contour_T (mm)	CMD between Marker_T and Contour_T (mm)	Difference (mm)
Max	15.8	9.1	8.3
Min	1.9	1.4	-0.9
Mean	6.6	3.9	2.7
SD	2.6	1.8	2.4

Table III. Percentage of the daily D95 of CTV with expansion less than 95% and 99% of the prescribed dose for the three registration methods.

	Percentage < 95%			Percentage < 99%		
CTV Expansion (mm)	Marker_TR	Marker_T	Contour_T	Marker_TR	Marker_T	Contour_T
0	4.7%	4.7%	0%	14.0%	7.0%	0%
2	27.9%	11.6%	2.3%	44.2%	20.9%	7.0%
4	58.1%	27.9%	4.7%	93.0%	60.5%	27.9%
6/4	88.4%	76.7%	67.4%	100%	97.7%	93.0%
6	95.3%	93.0%	72.1%	100%	100%	95.3%

Table IV. Systematic and random components (in degrees) of prostate rotations in literature.

Authors		Systematic Components			Random Components		
		LR	AP	SI	LR	AP	SI
Contour based registration	Van Herk et al.	N/A	N/A	N/A	4	1.3	2.1
	Stroom et al.	3.6	0.8	1.7	3.3	0.9	1.5
	Hoogeman et al.	5.1	1.3	2.2	3.6	1.6	2
Marker based registration	Dehnad et al.	4.7	2	2.7	3.6	1.7	1.9
	Aubry et al.	5.6	2.2	2.4	6.1	2	2.8
	Owen et al.	7.6	5	7.7	10.2	6.5	15.8
	Our study	4.6	2.3	2.1	4.1	2.0	2.0

FIG. 1. Prostate contours from different registration methods in (a) transverse, (b) coronal, and (c) sagittal views. Prostate contours in different colors are explained as follows: Prostate_Marker_TR is shown in blue; Prostate_Marker_T is shown in red; Prostate_Contour_T is shown in purple; and Prostate_CBCT is shown in yellow.

FIG. 2. Prostate rotational shifts (a) and its distributions (b).

FIG. 3. Center of Mass Distance (CMD). (a) CMD between the Prostate_Contour_T and Prostate_CBCT; (b) CMD between the Prostate_Contour_T and Prostate_Marker_TR, CMD between the Prostate_Contour_T and Prostate_Marker_T, and their difference.

FIG. 4. Overlap index (OI) as a function of CTV to PTV margin for a patient averaged over 5 fractions.

FIG. 5. The mean value of the daily CTV D95 versus CTV expansion margins for the three registration methods. Error bar represents one standard deviation. The p-value for the two marker registrations for each CTV expansion are also displayed.

FIG. 6. Percentage curve of the CTV D95 less than (a) 95% and (b) 99% of the prescribed dose as a function of the CTV expansion margins.

FIG. 7. Daily D5 and D50 of the bladder and rectum. Column represents mean value and error bar corresponds to one standard deviation. The p-value for the two marker registrations for each OAR dose are shown at top.

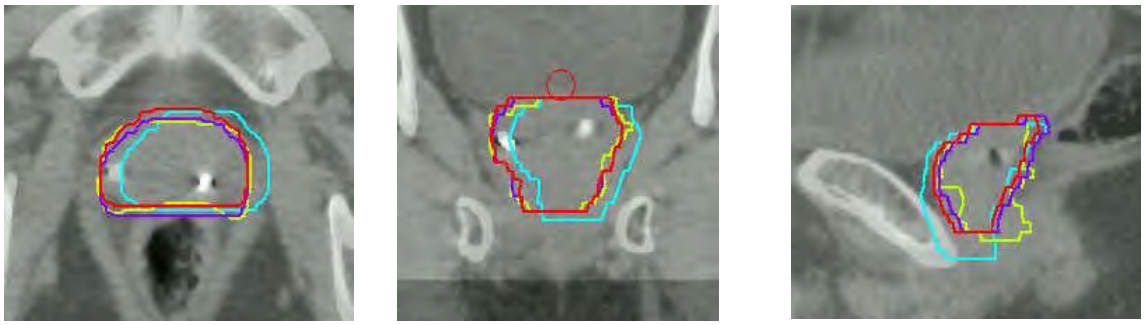

(a) (b) (c)

FIG. 1.

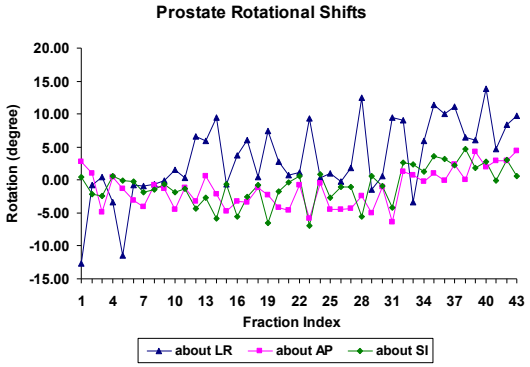
Prostate Rotational Shifts
Rotation (degree)
20.00
15.00
10.00
5.00
0.00
-5.00
-10.00
-15.00
1 4 7 10 13 16 19 22 25 28 31 34 37 40 43
Fraction Index
about LR
about AP
about SI

(a)

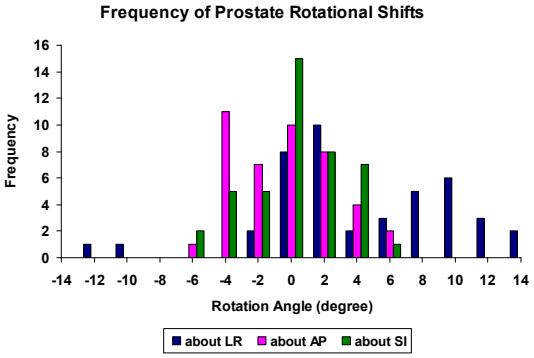
Frequency of Prostate Rotational Shifts
Frequency
16
14
12
10
8
6
4
2
0
-14 -12 -10 -8 -6 -4 -2 0 2 4 6 8 10 12 14
Rotation Angle (degree)
about LR
about AP
about SI

(b)

FIG. 2.

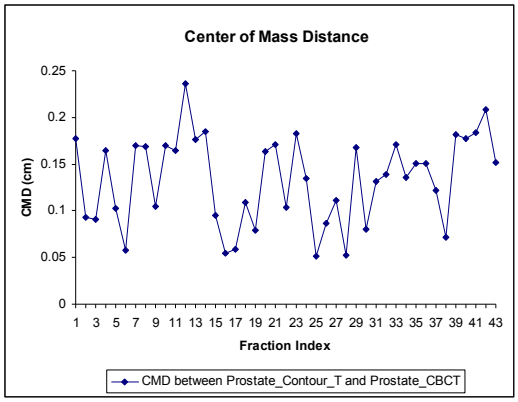
Center of Mass Distance
CMD (cm)
0.25
0.2
0.15
0.1
0.05
0
1 3 5 7 9 11 13 15 17 19 21 23 25 27 29 31 33 35 37 39 41 43
Fraction Index
CMD between Prostate_Contour_T and Prostate_CBCT

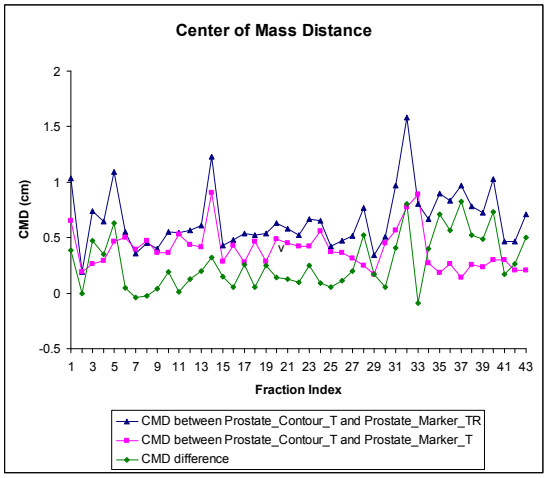
Center of Mass Distance
CMD (cm)
2
1.5
1
0.5
0
-0.5
1 3 5 7 9 11 13 15 17 19 21 23 25 27 29 31 33 35 37 39 41 43
Fraction Index
CMD between Prostate_Contour_T and Prostate_Marker_TR
CMD between Prostate_Contour_T and Prostate_Marker_T
CMD difference

(a) (b)

FIG. 3.

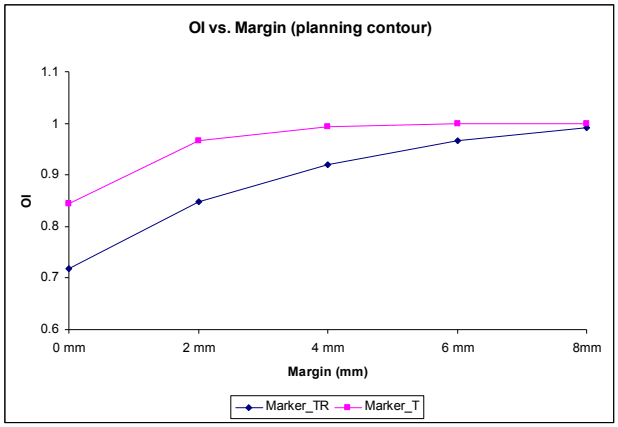
OI vs. Margin (planning contour)
1.1
1
0.9
0.8
0.7
0.6
OI
0 mm
2 mm
4 mm
6 mm
8mm
Margin (mm)
Marker_TR
Marker_T

FIG. 4.

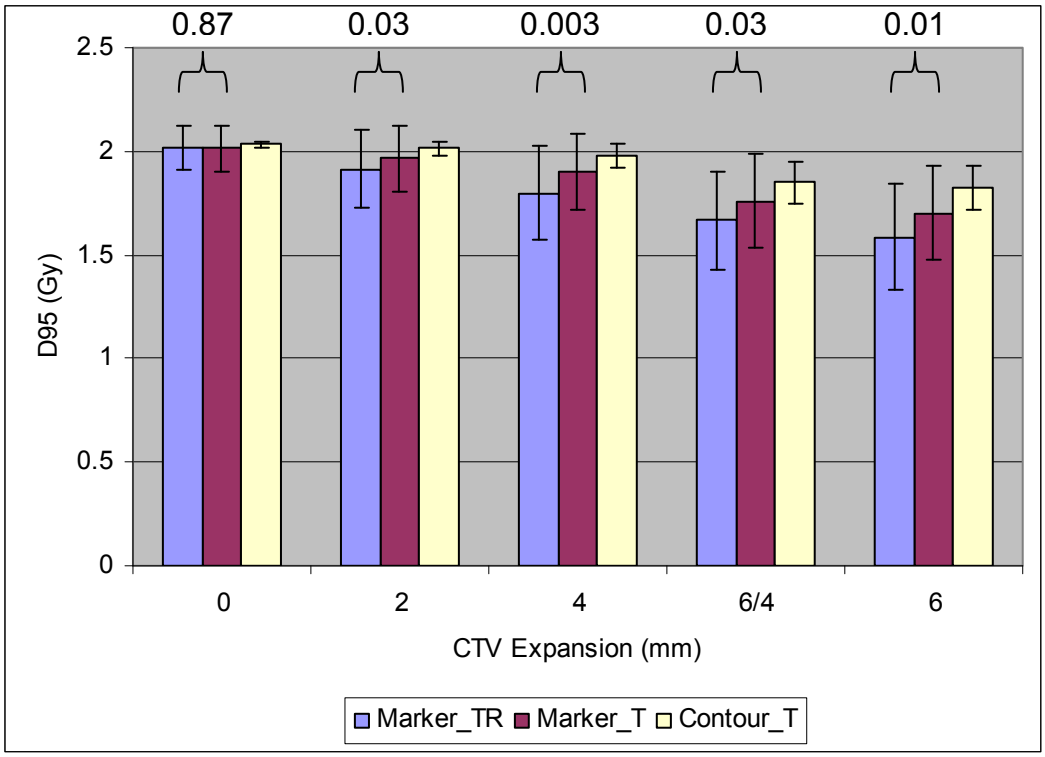
0.87
0.03
0.003
0.03
0.01
2.5
2
1.5
1
0.5
0
D95 (Gy)
0
2
4
6/4
6
CTV Expansion (mm)
Marker_TR
Marker_T
Contour_T

FIG. 5.

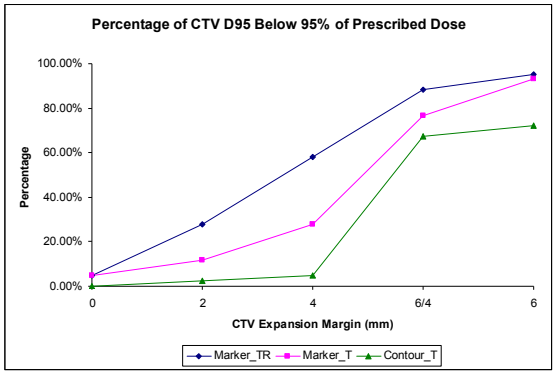
Percentage of CTV D95 Below 95% of Prescribed Dose
100.00%
80.00%
60.00%
40.00%
20.00%
0.00%
Percentage
0
2
4
6/4
6
CTV Expansion Margin (mm)
Marker_TR
Marker_T
Contour_T

(a)

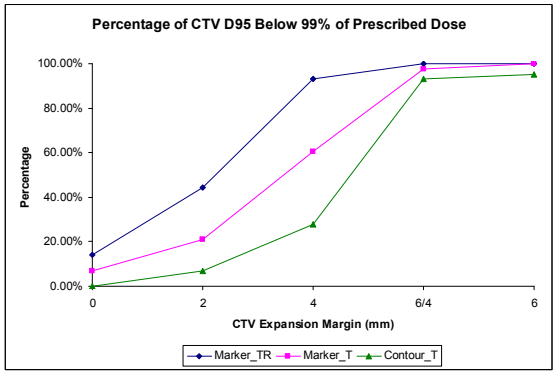
Percentage of CTV D95 Below 99% of Prescribed Dose
100.00%
80.00%
60.00%
40.00%
20.00%
0.00%
Percentage
0
2
4
6/4
6
CTV Expansion Margin (mm)
Marker_TR
Marker_T
Contour_T

(b)

FIG. 6.

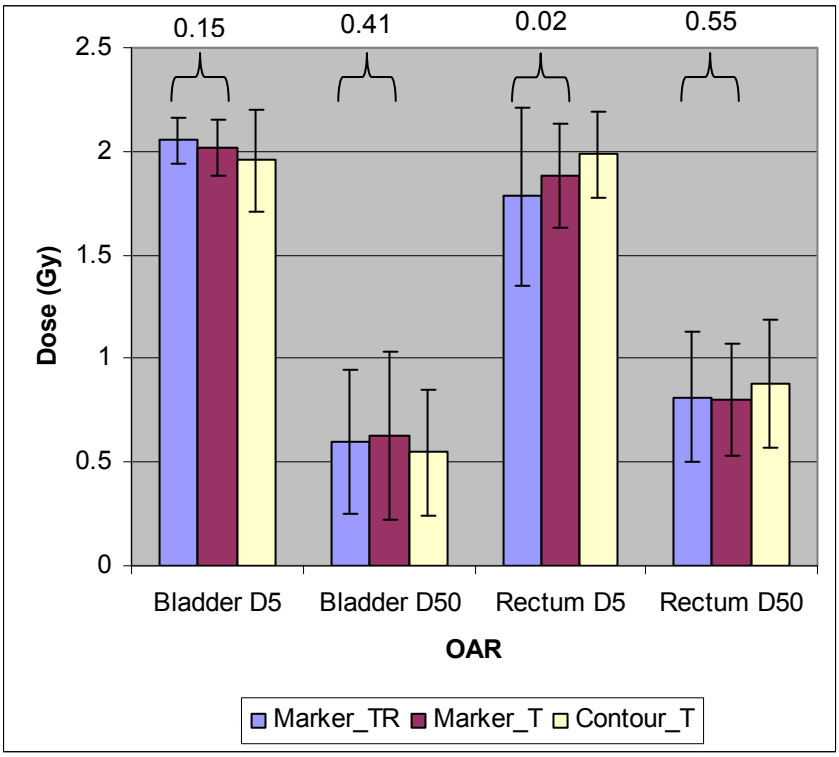
0.15
0.41
0.02
0.55
2.5
2
1.5
1
0.5
0
Dose (Gy)
Bladder D5
Bladder D50
Rectum D5
Rectum D50
OAR
Marker_TR
Marker_T
Contour_T

FIG. 7.

Appendix B

Evaluation of Atlas-Based Auto-Segmentation on Daily In-Room CT for Prostate Cancer

Wen Li[1], Yahua Zhong[2], Andrew Vassil[1], Ping Xia[1]

[1]Department of Radiation Oncology, Cleveland Clinic Foundation, Cleveland, OH

[2]Department of Radiation Oncology, Zhongnan Hospital, Wuhan, China

Short Title: Atlas-based auto-segmentation for prostate cancer

Word count: 3613

Address correspondence to: Ping Xia, Ph.D.

T2-028A

Cleveland Clinic Foundation

9500 Euclid Avenue

Cleveland, OH 44106

Tel: 216-444-1938

Fax: 216-444-8934

Email: xiap@ccf.org

Abstract

Purpose

Anatomy delineation is a major time consuming task to correct for inter-fractional changes in anatomy. Atlas-based auto-segmentation (ABAS) was developed to expedite this process. This study aims to evaluate the performance of ABAS applying to high quality verification CT-imaging acquired using a CT-on-rail system for prostate cancer.

Method

The prostate, rectum and bladder were manually contoured for seven prostate cancer patients. For each patient, three patient specific atlases were generated consisting of one, four and seven prior image and contour sets. ABAS was applied using these atlases for the last seven daily CT images of each patient. The auto- and manual-contours were compared both geometrically and dosimetrically. The reproducibility of the observation was validated by an experienced radiation oncologist performing the same procedure. The performance of ABAS with patient and non-patient specific atlases were also evaluated on 21 image sets. $P<0.05$ was considered statistical significant for two-tailed paired student *t*-test.

Results

Contours obtained from ABAS agreed well with the manual ones. With 1-image set atlas, the OI and DSC for the bladder were greater than 96% and 91%, respectively. Both indices were above 81% for rectum and prostate. The consistencies significantly improved by including 4 image sets in the atlas, while a further increase of atlas size to 7 did not show obvious benefits. Dose coverage for the auto- and manual-contours was similar for all organs. Similar results were obtained by the second observer. Compared with non-patient specific atlas, patient specific atlas yielded significantly more accurate contours. The time for ABAS and manual contouring was ~2 min and ~20 min per image set, respectively.

Conclusion

With diagnostic quality verification images, ABAS can provide fast and accurate delineations for prostate cancer on a daily basis. The inclusion of more than one CT set in atlas improves the contouring results.

Key Words: auto-segmentation; contouring; prostate cancer; CT-on-rail; re-planning

Introduction:

Modern radiation therapy techniques are geared towards conformal delivery to maximize the treatment effect for tumor and to minimize the radiation exposure for healthy tissues. This theoretical advantage, however, can be compromised by inter-fractional organ motions and deformations (1). Various image-guided radiation therapy (IGRT) approaches have been developed to correct such error (2, 3). The re-positioning method is prevalently used and it shifts the patient's couch based on the images acquired immediately before the treatment (2). However, such approach can not completely account for the rotational motions and organ deformations. Alternatively, adaptive re-planning was suggested to be able to provide a complete compensation for such changes (3, 4). However, the long re-planning time limits its application in clinical routines.

A major time consuming step for re-planning is the delineation of regions of interest (ROI), i.e., tumors and organs at risk (OAR). The contouring of a head and neck case and a prostate case generally takes 2 hrs and 30 mins, respectively (5). This long contouring time leads to both logistic and technical challenges (6). In addition, the manual contouring process is known to suffer from inter- and intra-observe variations (7). Recently, an atlas-based auto-segmentation (ABAS) method has been proposed that generates the new contours by deforming the prior contours to fit the anatomy of the new images (8). The improvement in contouring time and consistency has been demonstrated at different disease sites, i.e., prostate bed (6), head and neck (9), pelvis (10). In ABAS method, multi-image set atlas provides better results than the single-image set atlas since it contains images with greater geometric similarity to the new images. However, such advantage has not been exploited to the fullest extent because the images from most multi-image set atlases are from different patients due to the limited number of high quality CT images for each patient. This shortage of high quality image also limits the application

benefit of ABAS to a few sessions for each patient, i.e., the planning CT and/or a mid-treatment CT (10, 11).

Recently, in-room CT system such as CT-on-rail is increasingly used in clinical practices over the country (12). The availability of high quality daily images provides a new regime for the application of ABAS. First, it can be applied on a daily basis. As a result, patient-specific and multi-image set atlases can be developed, which may significantly improve the performance of ABAS as discussed above. However, few studies have explored these potential applications.

In the current study, we performed a thorough evaluation of ABAS on prostate cancer patients with daily CT acquired from a CT-on-rail system. The overall performance was evaluated both geometrically and dosimetrically by comparing the auto contours with the manual ones. The effect of including multiple and/or patient specific image sets in atlas was explored. The reproducibility was also validated by comparing the results with those obtained from a second observer.

Method

The current study was performed retrospectively on prostate cancer patients (n = 7), whose daily CT images were acquired using a CT-on-rail system. The contouring and analysis work was performed using a commercial software program, MIM 5.2 (MIMVista, Cleveland, OH). All procedures in the current study were approved by the institutional-review board at Cleveland Clinic Foundation.

The algorithm of the ABAS in MIM 5.2 has been described previously (6, 10, 11). Briefly, atlas is generated by including one or more CT images and their associated contours. The atlas image

sets are then compared with the new image set. The one with best geometrical similarity is selected. Subsequently, an intensity-based deformable registration is applied to map the contours of the selected image set to fit the anatomy of new images.

ABAS with single- and multi-image set atlases

To provide the dataset for atlas and the 'gold-standard' for contour comparison, all daily CT images were manually contoured based on the guidelines from Radiation Therapy Oncology Group (RTOG) 0126. Prostate, rectum and bladder were considered as the ROIs. To evaluate the effect of atlas size, three patient-specific atlases were generated for each patient using his/her first one, four and seven daily CT image sets and the associated manual contours. These atlases were subsequently applied to generate auto contours for the last seven daily CT image sets. The volumes of manually (V_m) and automatically (V_a) generated contours, as well as their intersectional areas, were recorded on a pixel-by-pixel basis. The accuracy of the auto contours was evaluated by their geometrical similarity to the manual contours using the dice similarity coefficient (DSC) and overlapping index (OI) as below:

$$DSC = \frac{2(Vm \cap Va)}{Vm + Va}$$

$$OI = \frac{Vm \cap Va}{Vm}$$

The dose distributions in the manual and auto contours were also compared. Bladder and rectum were evaluated using the absolute doses received by 5% (D5) and 50% (D50) of the volumes. For prostate, the D95 and D99 normalized by the prescription dose of each patient were used for comparison.

ABAS with Patient and Non-Patient Specific Atlases

To evaluate the effect of patient specific atlas, the above results were compared with those obtained from a non-patient specific atlas, which consisted of the first daily CT image set and

associated manual contours from four different prostate patients. Subsequently, ABAS was performed on the last seven daily CT image sets of three patients who were not included in the atlas. The DSC and OI were calculated as described above and compared with those obtained with 4-image set patient specific atlases.

Reproducibility of ABAS and Manual Contouring

To validate the performance reproducibility of ABAS, the ABAS study was repeated by an independent radiation oncologist. The manual contours for each patient were first regenerated. Patient specific atlas that consisted of the first daily CT image set and its associated manual contours was then used for auto-segmentation. The auto contours were compared with those drawn manually by the same radiation oncologist. The resultant DSC and OI were compared with those from the first observer.

In addition, the manual contours made by the two observers were compared to show inter-observer variance for a total of 49 image sets from the seven patients. The geometrical overlapping indices (DSC and OI) were then compared with the above ABAS results from the two observers.

Statistical Analysis

All results were expressed as mean±SD. Two-tailed paired student *t* test was used for both geometrical and dosimetric comparisons. Statistical significance was assigned at $P<0.05$.

Results

With the use of single-image set atlas, the automatically and manually generated contours of bladder were almost identical for all image slices. A few exceptions occurred when both prostate

and rectum were also presented (Fig. 1&2). As a result, the OI and DSC were at a high level of 96% and 91%, respectively (Table 1). For prostate, the disagreement between the auto and manual contours mostly occurred at their beginning and ending slices. For rectum, air bubbles were found to be another major cause for the inaccuracies in ABAS (Fig. 1). Nevertheless, an overall good agreement was observed. The OI and DSC were 84.6±5.5% and 82.5±6.4% for prostate, respectively. Although slightly lower, both of them remained above 80% for rectum.

The inclusion of multiple image sets in the atlas yields contours that were more consistent with the manual ones (Fig. 2). The use of four-image set atlas significantly improved the OI and DSC for prostate to 88.8±4.0% and 87.1±3.2%, respectively. Similar improvement was also observed for rectum. The OI and DSC were increased to 82.8±14.6% and 84.7±8.8%, respectively. The improvement in bladder contouring was not obvious since single-image set atlas already rendered superior results. An increase of atlas size to seven further improved the ABAS results for rectum. The OI and DSC were 86.2±9.2% and 87.8±9.9%, respectively. However, they did not show obvious benefits for bladder and prostate contours as compared with the four-image set atlas.

Despite of the differences in geometry, the dose distributions in manually and automatically generated ROIs were similar. The greatest difference was smaller than 4% and not statistically significant. These dosimetric differences did not show any correlation with the atlas size (Table 2).

Figure 3 shows the effect of patient specific atlas on ABAS's performance. For all ROIs, both DSC and OI were significantly better than those obtained with the non-patient specific atlas. Rectum exhibited the greatest differences in output (>40 %) in response to this change of atlas

components. The use of non-patient specific atlas decreased the DSC and OI from over 80% to a low level of 50.2±13.5% and 46.8±12.9%, respectively.

The reproducibility of ABAS's performance was validated by the second observer (Fig. 4). The DSC and OI were similar with those obtained from the first observer for all three ROIs, suggesting a strong reproducibility of the ABAS method. On the other hand, compared with the inter-observer variation in manual contours, ABAS yielded comparable geometrical similarity indices (< 3%) for both bladder and prostate. The ABAS generated indices (DSC: 81.0±6.7% and OI: 81.1±12.9%) were lower than the inter-observer variation (DSC: 87.5±4.5% and OI: 93.3±3.4%) for rectum because of the presence of air bubbles and large anatomical changes. These suggest that a manual 'fine tuning' process may significantly improve the contouring accuracy of rectum, while it is less critical for prostate and bladder.

On the workstation with a 3.07 GHz CPU and 12 GB RAM in our institution, the ABAS process took less than 2 min for each image set. This was over 7-fold faster than the manual contouring process, which took at least 15 min. Even when a manual 'fine-tuning' was performed on the auto contours, a significantly reduced contouring time (~5 min) was achieved.

Discussion

In the current study, the performance of the ABAS method was evaluated for prostate cancer on daily high quality CT image sets. The availability of patient specific and multi-image set atlas offered auto contours that agreed well with the manual counterparts. The reproducibility of this superior performance was validated by the second observer. These results suggest that ABAS can provide fast and accurate delineation for prostate cancer on a daily basis with the aid of CT-on-rail system.

Compared with previous ABAS studies (6, 9-11), a distinguish point of the current evaluation lies in the new designs of the atlas. Specifically, the availability of high quality daily CT images allows the use of early treatment sessions as the atlas database for ABAS on later treatment sessions. Therefore, patient specific and multi-image set atlas can be used. Both designs showed significant improvements in auto-segmentation (Table 1 and Fig. 3). This may be explained by the fact that the errors occurred during ABAS are positively related to the geometrical difference between the atlas image set and the new image set (8). Such difference is reduced without the individual variance for the patient specific design and/or with an increase in atlas size for the multi-image set design. However, it should be noted that such improvement is not boundless. Although an extremely large atlas database can theoretically contain all possible geometrical variations, the time to search through such database can be unbearably long. In addition, with a fixed number of treatment sessions for each patient, fewer sessions can benefit from the ABAS if more sessions are manually contoured to increase the atlas size. An atlas size of 4 appears to be the optimal choice in the current study (Table 1). Nevertheless, future investigations are needed for other disease sites and may provide further optimized choices.

The difference in the performance of ABAS for prostate, bladder and rectum is in line with the intensity based algorithm of the current ABAS method. For all three ROIs, the apex and base regions are relatively lack of signal contrast. Assuming these regions suffer from an equal inaccuracy in auto-segmentation, the difference in their portions with respect to the total volume would translate into the difference in the geometric similarity indices for each ROI. The less superior results for rectum may also be attributable to the presence of air bubbles. With lower signal intensity than the rectal tissues, the air bubbles can be easily mistaken as the rectal boundaries. Future development in the ABAS algorithm may address these problems. However,

this is beyond the scope of current study due to the corporate confidentiality agreement for our ABAS software (MIM 5.2).

It should be noted that the current study was designed to provide conservative evaluation for the performance of ABAS in daily practice. There was a long period (2~4 weeks) between the acquisition of the atlas image sets and the new image sets. Therefore, the geometrical difference between the atlas and new image sets were likely to be greater than that between any other image sets. Better results can be expected when ABAS is performed on image sets acquired earlier in the treatment course.

An immediate clinical application of the ABAS method is to lessen the burden on segmentation in off-line adaptive re-planning. Since only 'fine tuning' (~5 min) is needed to make auto contours clinically acceptable, over 3-fold of savings in time can be achieved. Such gain in efficiency would allow the performance of re-planning on more patients and therefore alleviate the shortage of radiation oncologist (13). It also allows the performance of re-planning on a more frequent basis for each patient, which would improve the sparing of the critical structures (14, 15). In addition, when combined with the fast dose calculation and optimization methods (3), it holds a great potential to advance the online re-planning practices to become a clinical routine.

The results of the current study have a particular impact on SBRT, which is increasingly used nowadays (16). To better spare the OARs, planning margin is commonly used. This, together with the escalated dose value and gradient, may cause devastating over/under dose effect when there are minor motions acceptable to conventional IMRT practice (17, 18). Therefore, re-planning would serve as a more critical means to compensate the inter-fractional motions (3). In

practice, multi-image set atlas may not be available due to the limited number of treatment sessions. Nevertheless, single-image set patient specific atlas appears to be adequate to yield satisfactory ABAS results (Table 1).

Conclusion

The performance of ABAS was explored in a new application setting provided by the in-room CT system. The use of patient specific atlas in ABAS generated auto contours that were high consistent with the manual ones. The inclusion of multi-image set in atlas showed further improvements. The time saved in contouring was significant even a manual 'fine tuning' after ABAS was counted. These results demonstrate the application potential of ABAS in re-planning to compensate inter-fractional motions on a wider and more frequent basis.

Acknowledgment

This research is supported in part by the United States Army Medical Research and Material Command (USAMRMC, PC073349) and in part by a research grant from Siemens Medical Solutions. The authors would like to thank Drs. Andrew Godley, Samah Ferjani, Han Liu and Qinyang Shang at Cleveland Clinic for insightful suggestions on the experiment design.

1. Sterzing F, Engenhart-Cabillic R, Flentje M, Debus J. Image-guided radiotherapy: a new dimension in radiation oncology. Dtsch Arztebl Int 2011;108(16):274-280.
2. Ruan D, Kupelian P, Low DA. Image-guided positioning and tracking. Cancer J 2011;17(3):155-158.
3. Ghilezan M, Yan D, Martinez A. Adaptive radiation therapy for prostate cancer. Semin Radiat Oncol 2010;20(2):130-137.
4. Mohan R, Zhang X, Wang H, Kang Y, Wang X, Liu H, Ang KK, Kuban D, Dong L. Use of deformed intensity distributions for on-line modification of image-guided IMRT to account for interfractional anatomic changes. Int J Radiat Oncol Biol Phys 2005;61(4):1258-1266.
5. Das IJ, Moskvin V, Johnstone PA. Analysis of treatment planning time among systems and planners for intensity-modulated radiation therapy. J Am Coll Radiol 2009;6(7):514-517.
6. Hwee J, Louie AV, Gaede S, Bauman G, D'Souza D, Sexton T, Lock M, Ahmad B, Rodrigues G. Technology assessment of automated atlas based segmentation in prostate bed contouring. Radiat Oncol 2011;6:110.
7. Mitchell DM, Perry L, Smith S, Elliott T, Wylie JP, Cowan RA, Livsey JE, Logue JP. Assessing the effect of a contouring protocol on postprostatectomy radiotherapy clinical target volumes and interphysician variation. Int J Radiat Oncol Biol Phys 2009;75(4):990-993.
8. Piper, J. Evaluation of an intensity-based free-form deformable registration algorithm. Med Phys 2007; 34(6): 2353-2354.

9. Han X, Hoogeman MS, Levendag PC, Hibbard LS, Teguh DN, Voet P, Cowen AC, Wolf TK. Atlas-based auto-segmentation of head and neck CT images. Med Image Comput Comput Assist Interv 2008;11(Pt 2):434-441.
10. Young AV, Wortham A, Wernick I, Evans A, Ennis RD. Atlas-based segmentation improves consistency and decreases time required for contouring postoperative endometrial cancer nodal volumes. Int J Radiat Oncol Biol Phys 2011;79(3):943-947.
11. Tsuji SY, Hwang A, Weinberg V, Yom SS, Quivey JM, Xia P. Dosimetric evaluation of automatic segmentation for adaptive IMRT for head-and-neck cancer. Int J Radiat Oncol Biol Phys 2010;77(3):707-714.
12. Ma CM, Paskalev K. In-room CT techniques for image-guided radiation therapy. Med Dosim 2006;31(1):30-39.
13. Erikson C, Salsberg E, Forte G, Bruinooge S, Goldstein M. Future supply and demand for oncologists : challenges to assuring access to oncology services. J Oncol Pract 2007;3(2):79-86.
14. Li AX. Adaptive Radiation Therapy. 2011.
15. Wu Q, Chi Y, Chen PY, Krauss DJ, Yan D, Martinez A. Adaptive replanning strategies accounting for shrinkage in head and neck IMRT. Int J Radiat Oncol Biol Phys 2009;75(3):924-932.
16. Ishiyama H, Teh BS, Lo SS, Mathews T, Blanco A, Amato R, Ellis RJ, Mayr NA, Paulino AC, Xu B, Butler BE. Stereotactic body radiation therapy for prostate cancer. Future Oncol 2011;7(9):1077-1086.
17. Mendez RA, Zinkstok RT, Wunderink W, van Os RM, Joosten H, Seppenwoolde Y, Nowak PJ, Brandwijk RP, Verhoef C, IJzermans JN, Levendag PC, Heijmen BJ. Stereotactic body radiation therapy for liver tumors: impact of daily setup corrections and

day-to-day anatomic variations on dose in target and organs at risk. Int J Radiat Oncol Biol Phys 2009;75(4):1201-1208.

18. Yin FF, Oldham M, Cai J, Wu Q. Dosimetry challenges for implementing emerging technologies. J Phys 2010;250(1):8-11.

Table 1. Geometrical comparison of the contours drawn manually and generated automatically with atlases containing different numbers of image sets.

		1-Image Set	4-Image Set	7-Image Set
Bladder	OI (%)	96.5±3.1*	95.5±2.7	95.9±2.8
	DSC (%)	91.4±5.0*†	93.6±4.3	94.8±2.5
Rectum	OI (%)	81.1±12.9†	82.9±14.3	86.2±9.1
	DSC (%)	81.0±8.7*†	84.7±8.6	87.6±14.6
Prostate	OI (%)	84.6±5.5*†	88.7±4.2	87.8±5.4
	DSC (%)	82.5±6.4*†	87.0±3.3	86.6±4.9

* $P<0.05$ compared to results from 4-image set atlas. †$P<0.05$ compared to results from 7-image set atlas.

Table 2. Dosimetric distribution in the ROIs drawn manually and generated automatically with atlases containing different numbers of image sets.

		Manual	1-Image Set	4-Image Set	7-Image Set
Bladder	D5 (Gy)	64.9±10.3	66.4±10.6	65.4±10.7	65.2±10.6
	D50 (Gy)	25.6±15.3	25.6±15.1	24.8±14.5	25.2±15.3
Rectum	D5 (Gy)	66.9±9.4	66.7±9.1	66.4±9.3	66.2±8.9
	D50 (Gy)	46.2±12.3	44.4±12.3	44.8±12.9	44.6±12.5
Prostate	D95 (%)*	99.6±2.0	99.6±1.9	99.6±1.9	99.6±1.8
	D99 (%)*	98.3±2.6	98.4±2.6	98.4±2.4	97.5±3.3

* D95 and D99 were normalized by the prescription doses.

Figure Legends

Figure 1. Manually and automatically generated contours on representative superior **(a)** and inferior **(b)** level slices. Single-image set patient specific atlas was used for ABAS.

Figure 2. Manually and automatically generated contours on a representative mid-level slice with prostate, bladder and rectum all presented.

Figure 3. Effect of the use of patient specific atlas for ABAS. DSC and OI were generated with four-image set atlas. * $P<0.05$ compared to results obtained using non-patient specific atlas.

Figure 4. Reproducibility study of ABAS methods. ABAS was performed with single-image set patient specific atlas. DSC and OI were obtained on the same 21 image sets from two independent observers. *$P<0.05$ compared to ABAS results from the 2nd observer. †$P<0.05$ compared to the inter-observer variations for manual contours. ‡ $P<0.05$ compared to the inter-observer variations for manual contours.

Appendix C:

Practical considerations of Multiple Adaptive Planning Strategy in Prostate Cancer Patients Receiving Whole Pelvis Radiotherapy

Peng Qi[1]*, Jean Pouliot [2], Mack Roach III[2], Ping Xia[1, §]

[1]Department of Radiation Oncology, Cleveland Clinic, Desk T28, 9500 Euclid Avenue, Cleveland, OH 44195
[2] Department of Radiation Oncology, the University of California at San Francisco, 1600 Divisadero Street, San Francisco, CA 94143

[§]Corresponding aurthor

Email addresses:
PQ: qip@ccf.org
JP: jpouliot@radonc.ucsf.edu
MR: mroach@radonc.ucsf.edu
PX: xiap@ccf.org

Abstract

Background
To resolve the challenge of concurrently treating the prostate and pelvic lymph nodes in whole pelvis radiotherapy (WPRT), we have proposed a new management strategy referred to as Multiple Adaptive Planning (MAP), in which a pool of treatment plans is created for the current and presumed prostate locations. According to daily prostate location, users select the most matched plan for the treatment of the day. We aimed at identifying the practical number of plans for implementation of the MAP technique by studying a larger group of patients.

Methods
Considering that large movements (>3 mm defined here) of the prostate relative to the pelvic bones are in the anterior/posterior (AP) and superior/inferior (SI) directions, we created 9 plans to accommodate prostate movements of 5 mm in one or two of these directions. From 33 fractions (of six patients), 17 fractions that demonstrated large prostate movements were selected for this study. For each fraction, one of 9 MAP plans was retrospectively selected according to the detected prostate movements, which were determined by dual image registrations: one aligned to the implant markers inside the prostate and the other aligned to the pelvic bones. The selected MAP plan was then applied to the corresponding MV cone beam CT (MV-CBCT) for dose calculation. For comparison, conventional isocenter shifting plans and retrospective adaptive plans were also created using MV-CBCT for each fraction. Three types of plans were compared in terms of dosimetric values of the targets.

Results
Of these fractions, the MAP, iso-shifting, and adaptive planning technique resulted in similar dose coverage to the prostate. Correspondingly, 95% of the prostate volume would receive a daily dose >97% of the prescription dose in 15, 16, and 17 fractions. The above techniques would result in 95% of the pelvic lymph node volume receiving a daily dose >97% of the prescription dose in 12, 6, and 17 fractions, respectively.

Conclusions
The use of the MAP technique with 9 pre-created plans can satisfy our treatment goals for WPRT treatment of prostate cancer with lymph node involvement.

Background

Although the use of whole pelvic radiotherapy (WPRT) in prostate cancer patients with pelvic lymph node involvement remains controversial, a growing body of data supports the role of this technique over that of prostate only RT (PORT) [1-9]. For WRPT, in which concurrent irradiation of the prostate and pelvic lymph nodes is required, IMRT can provide more advantages than 3D conformal radiotherapy (3D-CRT). These benefits include improved dose coverage to the lymph nodes and reduced toxicities to the rectum, bladder, and small bowel [10]. Therefore, IMRT has replaced 3DCRT and become the standard treatment modality for external beam WPRT.

Both designated as target volumes in WPRT, the prostate and pelvic lymph nodes have different movement patterns with respect to the pelvic bones: mobile for the former and fixed for the latter. Observed in previous studies, independent movements of the prostate vary from a few millimetres up to 1.5 cm relative to the pelvic bones [11-16]. It is also agreed that large prostate motions are not random, and they occur more often in the anterior/posterior (AP) and superior/inferior (SI) direction. Crook et al [11] showed that the base of the prostate was displaced more than 1 cm posteriorly in 30% of patients and in 11% in the inferior direction.

The relative movement of these two target volumes results in geometric configurations for treatment fractions different from those during CT simulation, and causes differences in delivery and planning doses. The magnitude of dose variations depends mainly on the use of image guidance, magnitude of prostate motions, and planning margins. With image-guided radiotherapy (IGRT) which is useful for treatments involving one target volume or multiple target volumes with fixed geometry, the discrepancy of delivered and planning dose was minimized. However, for concurrent treatments of two targets with varied geometric relationship, desired dose coverage for both targets is not guaranteed even under IGRT. For prostate only treatment, with 3 implanted markers as the imaging surrogates to identify daily prostate displacements, a common practice to correct for the prostate movement and setup errors is moving the treatment couch to match the daily and planning prostate locations. While preserving the prostate coverage, this method may compromise the nodal coverage when the prostate displacements are larger than the planning margins added on the pelvic lymph nodes. Although one can increase the planning margins to the pelvic nodes, the use of large margins increases doses to normal tissues and negates advantages of IMRT. The challenge of WPRT is to concurrently achieve dose coverage of the prostate and pelvic lymph nodes while using relatively small margins for both targets.

To resolve the above challenge for WPRT, an ideal approach is to create individual plan based upon daily images and contours for daily treatment, referred to as adaptive planning here. Although great efforts have been made to this strategy, it is now not clinically applicable. An alternative solution, referred to as MLC leaf-shifting method[17], has been proposed to compensate independent prostate movements by accordingly adjusting the positions of selected MLC leaf pairs (those only cover the whole or partial prostate) on the isocenter plane perpendicular to each beam angle. Although desired dose coverage of both targets can be achieved by using this MLC shifting approach, it is required to add a new feature in the record and verify (R&V) system for the clinical implementation. To circumvent this obstacle, we proposed another strategy referred to as multiple adaptive plan (MAP) IMRT[18] based upon a clinical case. The idea of the MAP technique is to create a pool of IMRT plans to accommodate multiple presumed prostate positions. With more presumed prostate positions included, dose coverage of both targets will be improved for the whole course of treatment. However, the MAP technique will be time-consuming and not practical as the number of prostate positions and accommodated IMRT plans are too big. In this study, we aim at identifying the practical number

of IMRT plans required for the clinical implementation of the MAP-IMRT technique based upon a larger group of patients. We retrospectively evaluated and compared this strategy with the iso-shifting and adaptive re-optimization strategy. The iso-shifting strategy here is the clinically implemented approach, which consists of shifting the treatment isocenter based on absolute prostate movements. The adaptive re-optimization strategy is to generate a new treatment plan using the daily contours while using the same treatment guideline as the original plan.

Methods

Planning

WPRT for prostate cancer patients includes two steps: an initial IMRT and a boost. Our study was based upon initial IMRT plans only. For the initial IMRT, primary treatment goals are to deliver a prescription dose of 45-54 Gy to the planning target volume (PTV) of the prostate and seminal vesicles (SVs) and to concurrently deliver a 45 Gy prescribed dose to the PTV of the pelvic lymph nodes over 25 fractions. The PTVs were created by expanding the prostate 1 cm (0.8 cm posteriorly) and the pelvic lymph nodes 0.5 cm in all directions.

Based on our planning protocol, a configuration of 7 (0°, 35°, 90°, 160°, 200°, 270°, and 315°) coplanar beams of 18 MV was used for all patients. All IMRT plans were created in the Pinnacle (v8.0, Philips, Andover, MA) treatment planning system (TPS) by using the direct machine parameter optimization (DMPO). In addition to meeting the treatment goals for all target volumes, other primary plan acceptance criteria included: keeping < 5% of the bladder and rectum from receiving the prescription dose to the prostate and < 20% of the bladder and rectum from receiving the prescription dose to the pelvic lymph nodes. We applied a proper normalization to D_{max} so that at least 95% of the PTVs were covered by the prescribed doses.

Dual image registration

All patients were treated on an Oncor (Siemens, Concord, CA) linear accelerator (linac). The modality for image-guidance equipped with the ONCOR linac was megavoltage (MV) cone-beam CT (CBCT). The MV CBCT system acquired images by using a 6 MV beam from the gantry and an amorphous silicon (a-Si) flat panel detector (AG9-ES, PerkinElmer Optoelectronics, Fremont, CA). Before a treatment, a CBCT acquisition field was added to the patient treatment using a pre-defined CBCT protocol. During the delivery of this CBCT field, one portal image was acquired for each degree during a 210° (from 270° to 100°, clockwise) gantry rotation. The image reconstruction started immediately after the acquisition of the first portal image, and a typical reconstruction volume is 256 × 256 × 274 (1.1 × 1.1 × 1.0 mm^3 in voxel size) [19],[20].

In clinical situation, the MV CBCT and planning CT images were registered based upon 3 gold markers implanted into the prostate gland (see Figure) using a commercial system (MVision™, Siemens Medical Solutions, Concord, CA). For our purpose, we performed a second image registration based upon the pelvic bony structures. Knowing the pelvic nodes relatively fixed to the pelvic bones, we derived the prostate displacement relative to the pelvic lymph nodes from the difference between the shifts of these two image registration procedures. The fractions showing large relative prostate shifts (>0.3 cm in any directions) were selected for this study.

The above dual image registration was also implemented in the Pinnacle TPS in which daily contours were generated and delivered doses the targets and OAR were retrospectively calculated. In practice, we first expanded clinical MV CBCT (256 × 256) to match the dimensions of the planning CT (512 × 512). Next, we sent these processed images to the Pinnacle system via DICON and used them as the primary image set. Afterwards, we imported

the planning CT (as the secondary image set) and associated contours into the same plan via DICOM. Successive image registrations between the planning CT and daily CBCT were performed by respectively aligning the implanted markers (see Fig. 1) and pelvic bones. Because rotational corrections were not explicit considered during treatment, rotational parameters for image registration were disabled during this image registration.

Creation of daily contours

To retrospectively compare and evaluate daily delivered doses to the target and OARs, daily contours based on MV CBCT were required. However, because of limited soft-tissue contrast in MV CBCT, it is nearly impossible to accurately contour the prostate and other organs on MV CBCT. Our current solution to this problem was to use the CT based contours as the template followed by possible modifications on certain slices in the Pinnacle TPS.

Considering independent motions of different organs, we transferred the original CT based contours to the daily CBCT through different image registration procedures. We transferred the prostate contour after a rigid image registration by aligning implanted markers inside the prostate. We then transferred the contours of the pelvic lymph nodes, body tissues, bladder, and rectum from the planning CT to MV CBCT after an image registration by aligning the pelvic bones. If large prostate shifts occurred, the bladder and rectum contours on the slices with prostate appearance were modified to avoid overlap or gaps between them and the prostate contour. In addition, when air appeared in the rectum on certain CBCT slices involving the prostate, we modified the rectum and prostate contour accordingly on those slices. After this step, we retrospectively simulated the daily anatomic structures on the daily MV CBCT.

MAP strategy

The MAP strategy requires that a pool of IMRT plans is created based on a planning CT and each plan is individually optimized to a presumed prostate location. The number of presumed prostate locations was determined by two factors: shift directions and the increment of shifts in each direction. In this study, we created prostate contours in consideration of only 4 directions (AP and SI) and 2 shifts (0 mm and 5 mm shift) in each direction using an in-house program. Therefore, the total number of plans in the MAP technique was 9, including the plan with no shifts, A5, P5, S5, I5, A5S5, A5I5, P5S5, and P5I5 (e.g. A5 stands for 5 mm in the anterior direction). The shifts in the left-right (LR) direction was excluded because prostate movements along the lateral direction were minimal, based on previous studies[11-16] and our observation. Though large shifts more than 1 cm have been observed, their occurrence was much lower than shifts from 0 cm to 1 cm. In this study, we chose 5 mm as the average shift in each direction. For each presumed prostate, an IMRT plan was created based on the guideline described in section II.D. Because we neglected setup errors and prostate distortions, we did not add margins to the prostate and pelvic lymph nodes. The constraints of the PTV were correspondingly changed to the prostate and pelvic lymph nodes for DMPO in the Pinnacle TPS. In the future, a small margin may be added to the targets in practice and it may leave for future investigation.

By registering implanted markers inside the prostate on daily CBCT and planning CT, we obtained the prostate displacements of the day in reference to the planned isocenter. According to these shifts, the treatment couch was moved to ensure the treatment isocenter for each treatment beam the same as the planned isocenter. This method is referred to as the iso-shifting technique. For this study, we simulated the couch-shifting through shifting the isocenter accordingly.

Based on daily contours, we also created an adaptive IMRT plan using DMPO in the Pinnacle TPS for each fraction demonstrating large prostate shifts, using the simulated daily contours and

the planning goals described in section II.B. Similar to the MAP technique, no planning margins were added to the prostate and pelvic lymph nodes of the day.

Relative dose comparison

We calculated doses using the daily MV CBCT in the Pinnacle TPS. However, the accuracy of such dose calculation is subject to the cupping artifacts and CT density inaccuracy as well as the limited FOV of our current MV CBCT imaging system. To circumvent these obstacles, we assigned a CT density of 1 g/cm^3 to all tissues enclosed by the external contour transferred from the planning CT. With these approximations, three sets of validation plans were generated on the daily CBCT using the MAP, iso-shifting, and adaptive planning strategy, respectively. The dose distributions in each plan were then analyzed and used for relative dose comparison among the MAP, iso-shifting, and adaptive planning strategy.

The isocenter, inside the prostate, in the planning CT was defined by the intersection of 3 fiducial markers on the patient's body. These markers were contoured and these contours were transferred to the daily CBCT along with the body (external) contour to help define the isocenter on the daily CBCT. The isocenter on the daily CBCT was shifted according the shifts based on the implanted markers for the iso-shifting plan and unchanged for the MAP and adaptive plan.

Results

Dual image registration

In treatment of 6 patients, MV CBCT was taken on weekly basis, and a total of 33 fractions were found from patient database. After we performed dual image registrations for each CBCT and the corresponding planning CT, we found large prostate shifts (> 3mm in any direction) occurred in 17 fractions. The distribution of large prostate movements was shown in Fig. 2. As expected, lateral movements were small and large shifts occurred in the AP and SI direction.

Dose comparison

Of these fractions, the MAP, iso-shifting, and adaptive planning technique resulted in similar dose coverage to the prostate. Correspondingly, 95% of the prostate volume would receive a daily dose > 97% of the prescription dose in 15, 16, and 17 fractions (see Fig. 3(a). The above techniques would result in 95% of the pelvic lymph node volume receiving a daily dose > 97% of the prescription dose in 12, 6, and 17 fractions, respectively (see Fig. 3(b)). We also calculated delivered doses to the bladder and rectum. The average doses to 5% and 50% of the bladder (D5, D50), relative to the planned endpoint doses, would be 93.7% (62.0%), 97.1% (63.2%), and 92.2% (62.9%), respectively. The average D5 (D50) of the rectum relative to the planned endpoint doses would be 92.9% (59.6%), 92.5% (58.7%), and 89.8% (55.8%), respectively.

Discussion

We retrospectively evaluated the MAP technique based on 6 patients receiving concurrent treatment of the prostate and pelvic lymph nodes under MV CBCT guidance. With the assumption of minimal prostate movements in the lateral direction, we created 9 MAP plans for each patient with 9 presumed prostate contours: the contour delineated on the CT and 8 contours created by rigidly shifting this contour in one or two directions (AP and SI) by 0 or 0.5 cm. Compared to the iso-shifting strategy, which has been clinically used correct prostate locations, the MAP technique with 9 IMRT plans achieved similar prostate coverage but improved node coverage. In contrast to the adaptive planning, the gold standard for this study, the MAP technique resulted in highly comparable dose coverage of both targets except for one patient. For this study, prostate deformation and intrafraction motion were ignored.

Because our MAP plans can not account for all possible prostate shifts, the dose coverage of the targets may be compromised in fraction with relative prostate shifts different from 0.5 cm (see Fig. 2), especially in occurrence of shifts more than 1 cm. This situation was in part due to no margins used for the targets when generating MAP plans. Adding suitable margins (though smaller than the clinical margins) to the targets may further improve dose coverage of the targets in MAP plans and will be left for future studies. With reduced margins, better OAR sparing was also expected.

In creation of 9 plans for the MAP strategy, the first plan required longer time than others. After a plan was created to meet all planning criteria, it can be used as the template for creating other plans with minor changes in constraints and contours. In practice, the average time for creating 9 plans was about 3-4 hours with a fairly fast Pinnacle station. As well, using scripting in the Pinnacle TPS can further expedite the whole process. Though the overall time in preparation of MAP plans was protracted, the dosimetric improvement can be critical in WPRT compared to conventional iso-shifting technique. As shown in study, dose coverage in adaptive plans was slightly better than those in corresponding MAP plans. The difference is expected to be reduced with suitable margins added to the prostate contours and/or appropriate adjustments for optimization constraints (i.e. higher minimum dose to the prostate). The overall time for the MAP technique should be similar to that for the adaptive planning technique if 1/3 fractions ($25/3 \approx 8$) require replanning. Instead of having plans ready beforehand as using the MAP technique, a plan is created after image guidance and before the treatment for the adaptive planning method to compensate daily anatomic changes. This could result in protracted machine time and great pressure on all clinical staff.

Although other methods has been proposed for concurrent treatment of the prostate and pelvic lymph nodes [17, 21], they were not currently practical, which is similar to the case of the adaptive planning. In our original study of MAP study, we created a pool of five plans to compensate for prostate movements of 0.5 and 1.0 cm in the posterior and superior directions for a specific patient. However, with more patients studied, we believed that we should add plans accommodating for prostate in the anterior and inferior directions. Given the fact that the occurrence of large prostate displacement (>1 cm) was low, we used 5 mm as the maximum shift. We believed that the MAP technique with 9 plans can achieve similar dose coverage and OAR sparing as the adaptive planning technique based on our current studies using MV CVCT. Considering the limitations of MV CBCT, future studies of using large FOV KV CBCT or daily CT (e.g. CT on rail) are recommended. As IMRT widely used for WPRT, the adequate node coverage was prone to the non-randomized large prostate shifts, which has been observed by many studies. To ensure dose coverage of the prostate and lymph nodes in WPRT, the MAP technique or other adaptive planning technique is highly recommended. The concept of the MAP technique could be potentially extended to other sites involving target volumes with independent motion patterns.

Conclusions

The proposed MAP strategy can be directly applied into clinical practice immediately although it may require extra effort in treatment planning. Using of the MAP technique with 9 pre-created plans, which accommodate for independent prostate shifts, can achieve treatment goals for the IMRT treatment of high-risk prostate cancer.

Competing interests and Acknowledgement

This research is supported by the United States Army Medical Research and Material Command (USAMRMC, PC073349)

References

1. Seaward SA, V Weinberg, P Lewis, B Leigh, TL PhillipsM Roach, 3rd. **Improved freedom from PSA failure with whole pelvic irradiation for high-risk prostate cancer**.*Int J Radiat Oncol Biol Phys* 1998; **42**:1055-62.
2. Roach M, III, M DeSilvio, C Lawton, V Uhl, M Machtay, MJ Seider, M Rotman, C Jones, SO Asbell, RK Valicenti, S Han, CR Thomas, Jr.WS Shipley. **Phase III trial comparing whole-pelvic versus prostate-only radiotherapy and neoadjuvant versus adjuvant combined androgen suppression: Radiation Therapy Oncology Group 9413**.*J Clin Oncol* 2003; **21**:1904-11.
3. Jacob R, AL Hanlon, EM Horwitz, B Movsas, RG UzzoA Pollack. **Role of prostate dose escalation in patients with greater than 15% risk of pelvic lymph node involvement**.*Int J Radiat Oncol Biol Phys* 2005; **61**:695-701.
4. Roach M, 3rd, M DeSilvio, R Valicenti, D Grignon, SO Asbell, C Lawton, CR Thomas, Jr.WU Shipley. **Whole-pelvis, "mini-pelvis," or prostate-only external beam radiotherapy after neoadjuvant and concurrent hormonal therapy in patients treated in the Radiation Therapy Oncology Group 9413 trial**.*Int J Radiat Oncol Biol Phys* 2006; **66**:647-53.
5. Spiotto MT, SL HancockCR King. **Radiotherapy after prostatectomy: improved biochemical relapse-free survival with whole pelvic compared with prostate bed only for high-risk patients**.*Int J Radiat Oncol Biol Phys* 2007; **69**:54-61.
6. Aizer AA, JB Yu, AM McKeon, RH Decker, JW ColbergRE Peschel. **Whole pelvic radiotherapy versus prostate only radiotherapy in the management of locally advanced or aggressive prostate adenocarcinoma**.*Int J Radiat Oncol Biol Phys* 2009; **75**:1344-9.
7. Milecki P, M Baczyk, J Skowronek, A Antczak, Z KwiasP Martenka. **Benefit of whole pelvic radiotherapy combined with neoadjuvant androgen deprivation for the high-risk prostate cancer**.*J Biomed Biotechnol* 2009; **2009**:625394.
8. Mantini G, L Tagliaferri, GC Mattiucci, M Balducci, V Frascino, N Dinapoli, C Di Gesu, E Ippolito, AG MorgantiN Cellini. **Effect of whole pelvic radiotherapy for patients with locally advanced prostate cancer treated with radiotherapy and long-term androgen deprivation therapy**.*Int J Radiat Oncol Biol Phys* 2011; **81**:e721-6.
9. Morikawa LKM Roach, 3rd. **Pelvic nodal radiotherapy in patients with unfavorable intermediate and high-risk prostate cancer: evidence, rationale, and future directions**.*Int J Radiat Oncol Biol Phys* 2011; **80**:6-16.
10. Wang-Chesebro A, P Xia, J Coleman, C AkazawaM Roach, 3rd. **Intensity-modulated radiotherapy improves lymph node coverage and dose to critical structures compared with three-dimensional conformal radiation therapy in clinically localized prostate cancer**.*Int J Radiat Oncol Biol Phys* 2006; **66**:654-62.
11. Crook JM, Y Raymond, D Salhani, H YangB Esche. **Prostate motion during standard radiotherapy as assessed by fiducial markers**.*Radiother Oncol* 1995; **37**:35-42.
12. Roeske JC, JD Forman, CF Mesina, T He, CA Pelizzari, E Fontenla, S VijayakumarGT Chen. **Evaluation of changes in the size and location of the prostate, seminal vesicles,**

bladder, and rectum during a course of external beam radiation therapy.*Int J Radiat Oncol Biol Phys* 1995; **33**:1321-9.
13. van Herk M, A Bruce, AP Kroes, T Shouman, A TouwJV Lebesque. **Quantification of organ motion during conformal radiotherapy of the prostate by three dimensional image registration**.*Int J Radiat Oncol Biol Phys* 1995; **33**:1311-20.
14. Beard CJ, P Kijewski, M Bussiere, R Gelman, D Gladstone, K Shaffer, M Plunkett, P CastelloCN Coleman. **Analysis of prostate and seminal vesicle motion: implications for treatment planning**.*Int J Radiat Oncol Biol Phys* 1996; **34**:451-8.
15. Stroom JC, PC Koper, GA Korevaar, M van Os, M Janssen, HC de Boer, PC LevendagBJ Heijmen. **Internal organ motion in prostate cancer patients treated in prone and supine treatment position**.*Radiother Oncol* 1999; **51**:237-48.
16. Zelefsky MJ, D Crean, GS Mageras, O Lyass, L Happersett, CC Ling, SA Leibel, Z Fuks, S Bull, HM Kooy, M van HerkGJ Kutcher. **Quantification and predictors of prostate position variability in 50 patients evaluated with multiple CT scans during conformal radiotherapy**.*Radiother Oncol* 1999; **50**:225-34.
17. Ludlum E, G Mu, V Weinberg, M Roach, 3rd, LJ VerheyP Xia. **An algorithm for shifting MLC shapes to adjust for daily prostate movement during concurrent treatment with pelvic lymph nodes**.*Med Phys* 2007; **34**:4750-6.
18. Xia P, P Qi, A Hwang, E Kinsey, J PouliotM Roach, 3rd. **Comparison of three strategies in management of independent movement of the prostate and pelvic lymph nodes**.*Med Phys* 2010; **37**:5006-13.
19. Morin O, A Gillis, J Chen, M Aubin, MK Bucci, M Roach, 3rdJ Pouliot. **Megavoltage cone-beam CT: system description and clinical applications**.*Med Dosim* 2006; **31**:51-61.
20. Pouliot J, A Bani-Hashemi, J Chen, M Svatos, F Ghelmansarai, M Mitschke, M Aubin, P Xia, O Morin, K Bucci, M Roach, III, P Hernandez, Z Zheng, D HristovL Verhey. **Low-dose megavoltage cone-beam CT for radiation therapy**.*Int J Radiat Oncol Biol Phys* 2005; **61**:552-60.
21. Hsu A, T Pawlicki, G Luxton, W HaraCR King. **A study of image-guided intensity-modulated radiotherapy with fiducials for localized prostate cancer including pelvic lymph nodes**.*Int J Radiat Oncol Biol Phys* 2007; **68**:898-902.

Figures

Figure 1. MV CBCT and CT

Coronal view of MV CBCT and planning CT. Two gold seeds can be seen on this slice.

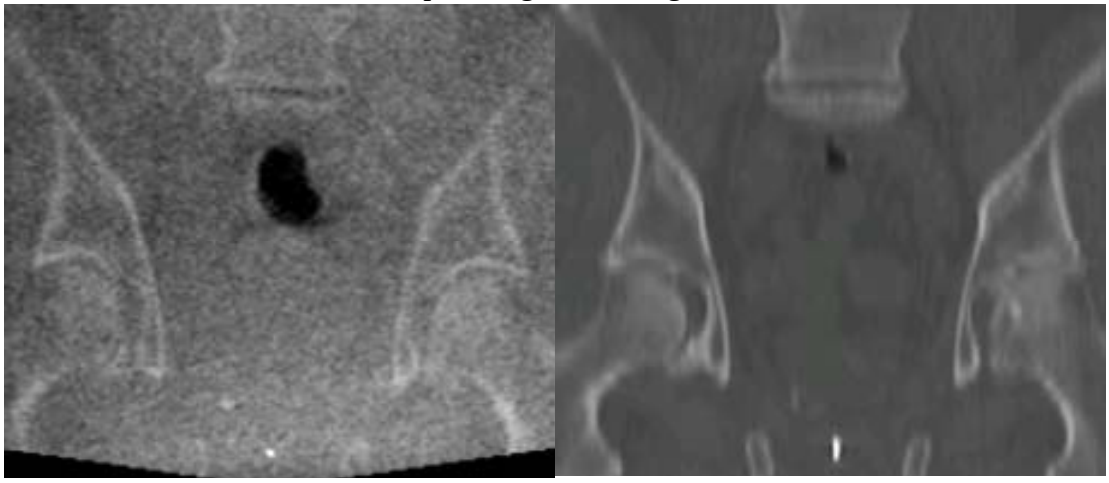

Figure 2 - Prostate shifts

Prostate shifts relative to the pelvic bones (lymph nodes) in 17 fractrions.

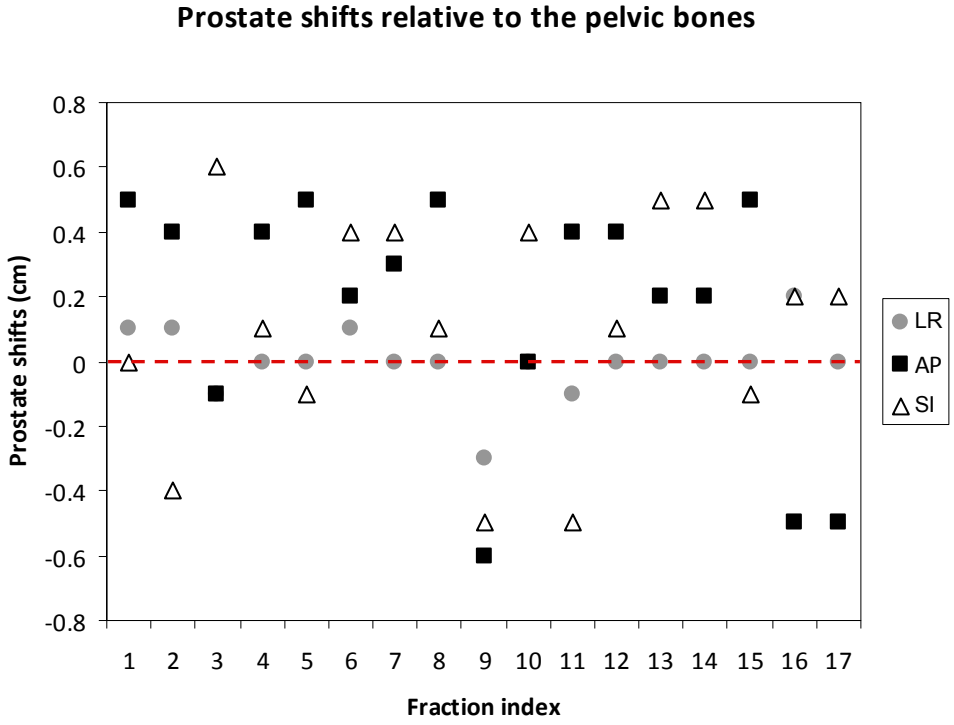

Figure 3 - Prostate coverage

(a) Prostate coverage and (b) Lymph node coverage in 3 types of IMRT plans.

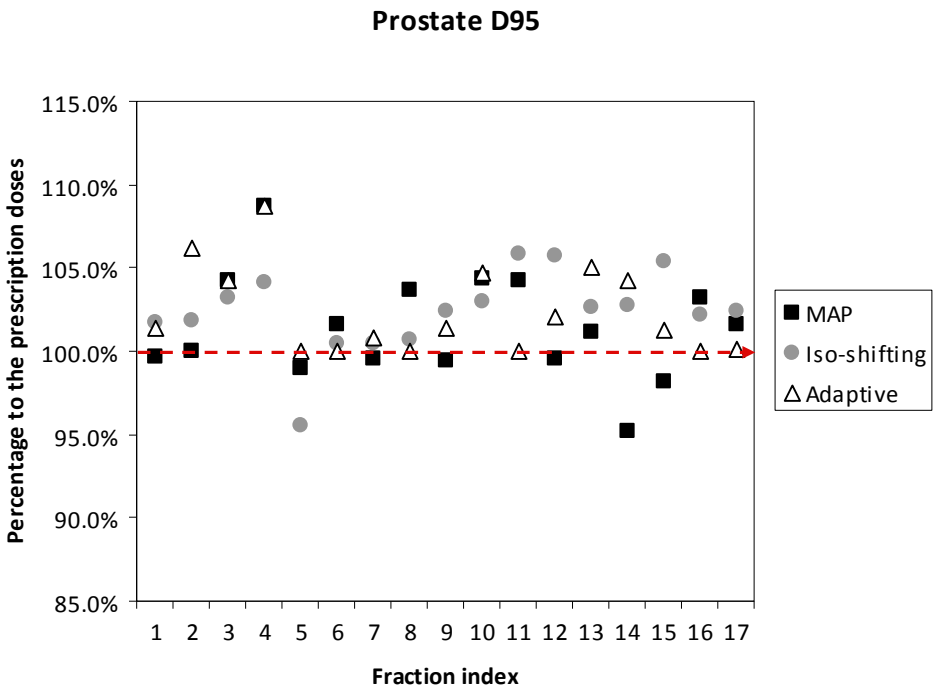

(a)

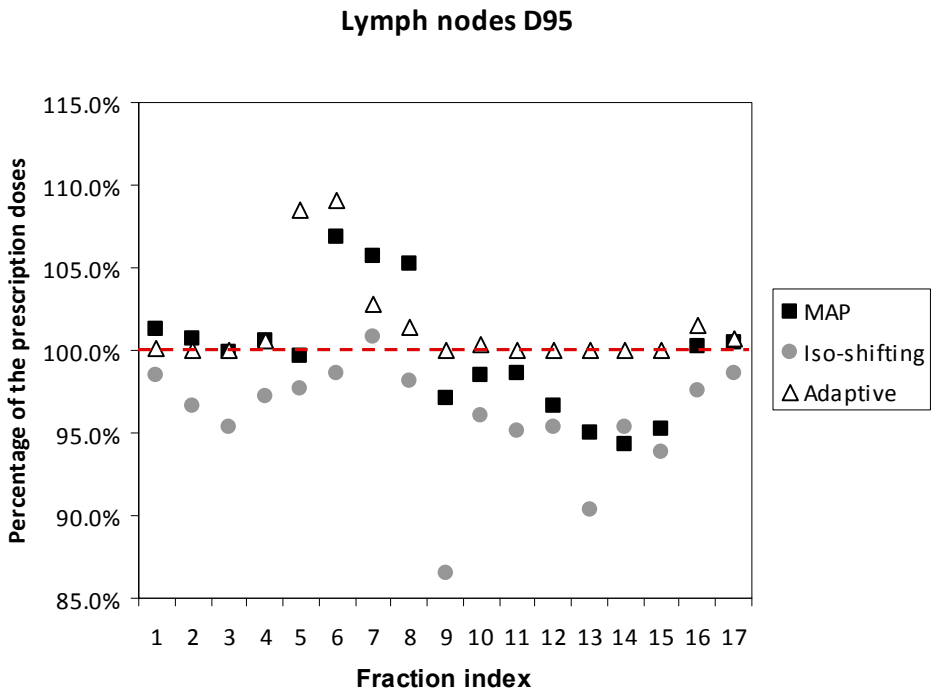

(b)

Tables

Table 1 MAP-IMRT plans and its usage for 17 fractions with shifts 0.4-0.8 cm.

Plan	A	P	S	I	AS	AI	PS	PI

Usage	6	2	5	0	1	2	0	1

Appendix D:

Accepted as a poster presentation at the Annual Meeting of American Association of Physicists in Medicine at Vancouver, BC, Canada, July 31-August 4, 2011. .

Daily Prostate Rotation should be Compensated in Translational Correction and not to be Ignored

Qingyang Shang, Lawrence Sheplan, Kevin Stephans, Rahul Tendulkar, and Ping Xia

Purpose: To quantify magnitude of the prostate rotation during daily treatment and evaluate strategies to effectively compensate the rotation if a six-degree table is not available.

Method and Materials: Six patients, with forty-four kilo-voltage cone beam CT (KV-CBCT), were selected for this study. On these KV-CBCTs, the prostate was contoured by a physician. These patients had three transponders implanted for non-imaging daily prostate localization using the Calypso system. To determine the prostate movement, we registered each KV-CBCT with the planning CT in four different ways: (a) manually align to the bones with translation only (Bone_T); (b) automatically align to the markers with both translation and rotation (Marker_TR); (c) manually align to the markers with translation only (Marker_T); (d) manually align to the prostate contour with translation only (Contour_T). The prostate rotations from the second method were recorded. Using the contour registration as a benchmark, two center of mass distances (CMD) between the Contour_T and Marker_TR/Marker_T registrations were calculated. Only translations were used for the CMD calculation.
Results: Detected from the Marker_TR method, the mean and standard deviation of the prostate rotations about the transverse, anterior-posterior, and longitudinal axes were 3.21±6.26°, -1.39±2.91°, and -0.94±2.75°, respectively. The mean CMD between the Contour_T and the Marker__TR/Marker_T shifted prostate were 6.6 and 4.0 mm, respectively. When the rotation is greater than 10°, the differences in CMD were greater than 5 mm in 7 out of 8 (87.5%) of such fractions. When the rotation is greater than 6°, the differences were greater than 4 mm in 13 out of 19 (68.4%) cases.

Conclusions: Without a six-degree table, prostate rotations were often not corrected. Compensating for the rotations with translational shifts is effective, and superior to ignoring rotations. Simply ignoring large rotations may lead to increased planning margins or inaccurate prostate localization.

Appendix E

Accepted as poster presentation at the Annual Meeting of American Association of Physicists in Medicine at Vancouver, BC, Canada, July 31-August 4, 2011.

Assessing Planning Margins Using Shifting Dose Matrix Method to Calculate Daily and Cumulative Doses Under Imaging Guided Radiotherapy (IGRT)

Guangshun Huang, Naichang Yu, Kevin Stephans, Rahul Tendulkar, and Ping Xia

Department of Radiation Oncology, Cleveland Clinic, Cleveland, OH 44195

Purpose: Under daily IGRT, treatment planning margins can be significantly reduced. To evaluate effectiveness of the current empirical planning margins, we developed an efficient method to assess daily and cumulative doses.

Methods and Materials: Under daily kilo-voltage cone beam CT (KV-CBCT), daily dose can be calculated directly using the CBCT, but this method is cumbersome and not necessarily accurate due to fluctuation of the CT numbers. Based on the Computational Environment for Radiotherapy Research (CERR) software, we developed additional MATLAB codes to shift the planning dose matrix according to the daily shifts detected by IGRT. Because the shifted dose matrices were in the same coordinate system, cumulative dose can be obtained by simple summation. For 20 patients with prostate cancer, the planning margin of 4 mm posterior and 6 mm elsewhere were utilized. For these patients, we calculated the daily doses and cumulative doses with and without IGRT to assess sufficiency of planning margins. The calculated composite delivery doses were compared to the planning doses for the prostate and the planning target volume (PTV).

Results: For the 20 cases examined, the dose differences to 95% of the prostate (D95) between the delivered and planned dose were from -3.5% to 0.4% (mean -0.1%). For the PTV, the differences in D95 were from -11.2% to 0.0% (mean -1.8%). The dose differences to the 50% of the rectal and bladder were from -5.2% to 13.2% (mean 3.1%) and from -19.6% to 1.0% (-5.0%), respectively.

Conclusion: The composite dose of multiple-fraction treatment can be obtained by using the shifting dose matrix method. Because of the adequate planning margin, the cumulative dose changes due to the prostate motion are small, even without IGRT, indicating either the planning margin can be reduced or the frequency of the IGRT can be reduced.